International Journal of Greenhouse Gas Control 146 (2025) 104453

Contents lists available at ScienceDirect

International Journal of Greenhouse Gas Control

journal homepage: www.elsevier.com/locate/ijggc

Study of an alternative route for alumina production: Integration of calcium looping to Pedersen process aiming at zero emissions and bauxite residue avoidance

Javier Sáez-Guinoa [a,b], Eva Llera-Sastresa [b], Luis M Romeo [a,b,*]

[a] Aragon Institute for Engineering Research (i3A), Campus Río Ebro I+D+i, Mariano Esquillor s/n, 50018 Zaragoza, Spain
[b] School of Engineering and Architecture, University of Zaragoza, Campus Río Ebro, María de Luna 3, 50018 Zaragoza, Spain

ARTICLE INFO

Keywords:
Alumina
Pedersen process
CO_2 capture
Pig iron
Calcium looping
Bauxite residue

ABSTRACT

The aluminium industry is a notable emitter of CO_2 and a significant contributor to mineral scarcity. Alumina extraction, typically conducted via the Bayer process, faces two main challenges: using fossil fuels and generating bauxite residue. A recently proposed approach, the Pedersen process, aims to address these challenges by removing the iron oxide content from the ore through an additional iron smelting step, thereby eliminating the generation of bauxite residue. This study evaluates the material and energy performance of alumina and pig iron co-production from bauxite using the principles of the Pedersen process. Different thermodynamic simulations of a Pedersen process layout were carried out using Aspen Plus software, and key parameters were validated against existing literature. Additionally, diverse CO_2 capture configurations based on calcium looping were assessed, performing an energy optimization to achieve carbon-neutral and zero-residue alumina production.

Results indicate that the energy demand of the Pedersen process is notably higher than the average Bayer process for bauxites with high aluminium/iron ratios, with an estimated energy consumption of 11.92 GJ per tonne of products. However, low aluminium/iron ratios render better energy performances (10.15 GJ per tonne), showing potential feasibility in terms of energy consumption. The integration of a calcium-looping plant led to low energy penalties, thanks to the replacement of $CaCO_3$ in the Pedersen plant by adding purged CaO from the calcium-looping plant. The energy penalties, estimated at a minimum of 1.10-2.79 GJ per tonne of CO_2 avoided, show favourable results that could pave the way for a smarter use of resources and a decarbonized alumina production.

1. Introduction

The European Union Commission has set forth objectives to significantly reduce greenhouse gas emissions and decouple economic growth from resource use, with the ultimate goal of achieving carbon neutrality by 2050 (The European Green Deal - European Commission). To accomplish these objectives, it is crucial to explore innovative technologies and mitigation strategies within the industrial sector, which is estimated to be responsible for approximately 24% of global CO_2 emissions (International Energy Agency 2020) and plays a significant role in resource consumption (United Nations Environment Programme 2024). Aluminium is one of the most widely used metals, with its primary production process accounting for 2% of total global CO_2 emissions (Saevarsdottir et al., 2020), equivalent to approximately 1.1 Gtonnes of CO_2 per year (International Aluminium Institute [IAI]). Alumina (Al_2O_3) is the essential precursor for primary aluminium industrial production. The growing demand for aluminium in recent years has led to a significant increase in alumina production, which exceeded 140 million metric tonnes worldwide in 2023 (International Aluminium).

Alumina extraction involves the digestion of the bauxite mineral in a caustic solution, dissolving aluminium ions, which are later crystallized to precipitate aluminium hydroxide, and subsequently calcined to produce alumina. The remaining caustic solution is then concentrated via an evaporation step, and the liquid is recycled back to the digestion of the rock. This overall process, known as the Bayer process, faces two major drawbacks: the generation of bauxite residue and the high energy requirements.

* Corresponding author.
E-mail address: luismi@unizar.es (L.M. Romeo).

https://doi.org/10.1016/j.ijggc.2025.104453
Received 18 June 2024; Received in revised form 14 August 2025; Accepted 14 August 2025
Available online 21 August 2025

The solid residues from the undissolved bauxite, commonly known as red mud or bauxite residue, typically account for more than 50% of the mineral input (Zhou et al., 2023). Bauxite residue is composed of iron oxides, unreacted aluminium oxides, caustic liquor and minor impurities such as calcium, silicon and titanium oxides. The generation of bauxite residues poses significant environmental impacts and health risks due to their highly alkaline content (Evans, 2016). These residues, usually disposed of in landfills near alumina refineries (Liu et al., 2009), easily penetrate soil, farmland and lakes, causing soil salinization and polluting surface water sources (Li et al., 2024). Therefore, the cumulative generation of bauxite residue, estimated at 4.6 billion tons in 2018 (Kar et al., 2023), encourages the search for solutions that enable the valorisation of this residue. Existing alternatives include the use of bauxite residue in cement production (Salim et al., 2023), soil amelioration (Holanda et al., 2020), and the recovery of alumina (Kar et al., 2023), other metals (Pilla et al., 2024) and rare earth elements (Swain et al., 2022). However, the alkalinity of the residue hampers its full utilization, limiting its application to 2-3% of the current bauxite residue produced (da C. Leite et al., 2022). Therefore, minimising or eliminating bauxite residue generation is imperative to guarantee efficient resource use and achieve circularity.

In parallel, efforts are also being directed toward reducing the energy consumption of the process and the greenhouse gas emissions associated with the use of fossil fuels. The demanding temperatures above 1100°C for the calcination of aluminium hydroxide are the main energy requirement of the alumina industry, followed by the thermal energy necessary for the evaporation and digestion stages (Sáez-Guinoa et al., 2024). Altogether, alumina production was estimated to require around 10.2 GJ of thermal energy per tonne produced in 2022 (Metallurgical Alumina Refining Energy Intensity - International Aluminium Institute). Strategies for alumina refineries to reduce energy consumption are primarily based on the direct electrification of low-temperature stages such as digestion and evaporation (International Energy Agency 2023, Alcoa to investigate low emissions alumina - Australian Renewable Energy Agency (ARENA), Alcoa – Refinery of the Future). However, the high temperatures and the elevated energy needed hinder a wider implementation of direct electrification in the alumina industry. Alternatively, other strategies to minimize CO_2 emissions, such as carbon capture and storage technologies, are still under development in alumina production, with no current industrial application. Nonetheless, some published works have studied its potential implementation. A conventional amine-based carbon capture system was proposed to minimize CO_2 emissions from alumina production (Peppas et al., 2023), showing the potential of a 65.3% reduction in direct CO_2 emissions across the entire aluminium production chain. A calcium-looping configuration was also proposed and evaluated following the methodologies of Life Cycle Assessment and Life Cycle Costing (Sáez-Guinoa et al., 2024). The results of the study showed a 7% increase in the energy consumption of an average alumina refinery while achieving the capture of 95% of direct CO_2 emissions, drastically reducing the overall environmental impacts and enhancing the economic performance thanks to the avoidance of CO_2 emission taxes.

1.1. Pedersen process

The Pedersen process is a proposed alternative to avoid generating bauxite residue (Pedersen, 1927).This process was applied industrially in Norway from 1928 to 1969, when it was discontinued for economic reasons (Georgala et al., 2023). However, the process has regained interest from research groups and authors in recent years, both as a method for primary alumina production from bauxite and for recovering alumina from bauxite residue (Kar et al., 2023). The key feature of the Pedersen process is the use of an electric arc furnace to remove the iron present in bauxite by smelting-reduction before extracting alumina from the rock. The reduced iron can be commercialized as pig iron, minimizing bauxite residue during alumina production. Alumina is obtained by leaching of calcium-aluminate slags in a Na_2CO_3 solution, followed by the precipitation of aluminium hydroxide using CO_2 as feedstock. The use of $CaCO_3$ and CO_2 leads to the generation of a residue known as grey mud, a sludge containing $CaCO_3$ and other impurities present in bauxite, such as silicon, titanium, aluminium and magnesium oxides. Despite the generation of this residue, the Pedersen process offers a promising solution regarding the problematic of bauxite residue management, as the grey mud residue contains fewer caustic or highly alkaline components, reducing its risk of soil and water contamination, making it a safer option for handling and long-term disposal (Dentoni et al., 2014). Moreover, grey mud typically has a more stable chemical composition than bauxite residue, making it easier to handle, and potentially repurpose in construction materials or soil amendments (Azof et al., 2020). As a matter of fact, several authors refer to grey mud as a by-product rather than waste, due to its many potential uses and benefits over bauxite residue (Azof et al., 2020, Ma et al., 2022, Vafeias et al., 2018).

A simplified flowsheet of the process is shown in Fig. 1, in which bauxite is initially dehydrated with $CaCO_3$ to allow the formation of calcium-aluminate slags during the reduction of iron in an electric arc furnace. Subsequently, the slag is pulverized to ease its digestion in Na_2CO_3 solution, where aluminium is dissolved and precipitated calcium carbonate is obtained. Finally, gaseous CO_2 is sparged into the solution containing aluminium ions, triggering the regeneration of Na_2CO_3 and the precipitation of aluminium hydroxide, which is later calcined to produce alumina.

Several authors have conducted different experiments over the last decade at laboratory scale to demonstrate the feasibility of alumina and pig iron co-production from bauxite, to gain a deeper understanding of the process fundamentals. The removal of up to 99.9% of iron ore content from low-grade bauxites using coke was demonstrated by Azof et al. (Azof et al., 2018), for which three different trials using 1-1.5 kg of bauxite were performed, also achieving partial separation of silicon and titanium. Safarian and Kolbeinsen (Safarian & Kolbeinsen, 2016) also completed iron removal in a smaller-scale experiment with commercial bauxite, indicating that more than 10% of the silicon dioxide contained in the ore was reduced together with iron. Sellaeg et al. (Sellaeg et al., 2017) also completed the removal of iron in three different tests, showing relevant differences in the phases of the calcium-aluminate slags produced depending on the lime addition. Although positive results regarding iron separation are achieved in the works reported in literature, their procedures show some mismatches with respect to the published data of the former industrial process (Miller and Irgens, 2013). Most of the experimental procedures perform the dehydration of bauxite and then mix it with commercial calcium oxide due to the low scale of the experiments conducted (usually in the range of 100-1,000 grams of bauxite), whereas the original industrial process co-processed both materials (bauxite and limestone) for cost savings. Additional experiments in larger or semi-industrial scales should confirm the technical viability of the process and bring it closer to commercialization. Lazou et al. (Lazou et al., 2020) carried out the smelting reduction of 100 grams of bauxite using hydrogen at different temperatures to minimize carbon emissions at this stage. Although iron reduction was feasible at lower temperatures, the substantial hydrogen demand required for its implementation may hinder the substitution of coke with hydrogen.

For downstream stages of the Pedersen process, Georgala et al. (Georgala et al., 2023) studied the aluminium digestion after iron removal using calcium-aluminate slags to extract alumina in a 0.6 L vessel containing Na_2CO_3 solution. The obtained recovery rate of aluminium after digestion was greater than 85% in all the experiments, attaining 95% recovery rates when using a 20% excess of slag at 95°C. Experimental tests within the ENSUREAL H2020 project (Konlechner et al., 2021) also obtained recovery rates of around 80% of aluminium after Na_2CO_3 digestion, whereas the efficiency of the subsequent precipitation reached over 99%. The leachability of the slag after iron removal is the limiting step of the process, presenting a wide range of results depending on the digestion conditions and the initial phases of

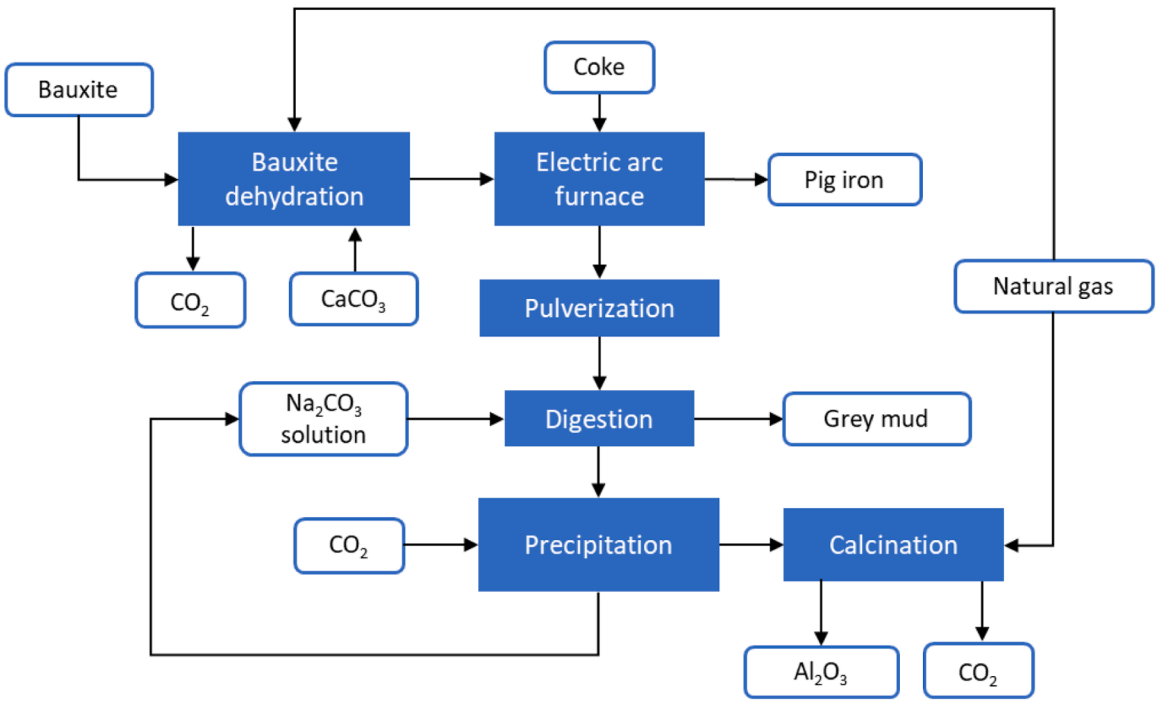

Fig. 1. Simplified flowsheet of Pedersen process for the co-production of alumina and pig iron from bauxite.

the calcium-aluminate slags (Azof et al., 2020).

Contrary to experimental studies, technical and environmental assessments of the global Pedersen process are scarcely found in the literature. Ma et al. compared both the Pedersen and Bayer processes (Ma et al., 2022), concluding that although the former has a higher energy demand, environmental impacts depend mainly on the carbon intensity of the energy used and the composition of the initial bauxite. Notably, no source of CO_2 feedstock has been provided in any of the available literature to date. Practical challenges from iron reduction and slag digestion restrict the focus on technical studies that analyse the CO_2 emissions and carbon supply system of the overall process.

1.2. Calcium looping

CO_2 capture technologies have gained significant interest due to their contribution to mitigating global warming. Among these technologies, calcium looping technology, also known as carbonate looping, has been on the focus of researchers for over 20 years (Greco-Coppi et al., 2025) since it was initially proposed by Shimizu et al. (Shimizu et al., 1999). Calcium looping (CaL) is one of the most promising alternatives of post-combustion carbon capture due to its relatively low energy penalty, estimated at 6-8 efficiency points in power plants (Romeo et al., 2008, Haran et al., 2023) and 2-5 GJ per tonne of CO_2 avoided in energy-intensive processes (Perejón et al., 2016, Ortiz et al., 2016), or even lower in highly integrated systems (Romeo et al., 2011).

CaL technology involves passing CO_2-rich combustion gases from a system through a carbonation-calcination cycle. Calcium oxide (CaO) is used as a sorbent to capture CO_2, forming calcium carbonate ($CaCO_3$) in a carbonation unit. This $CaCO_3$ is later decomposed in a calciner, and CaO is recycled back to the carbonation unit. CaL systems have been successfully tested in pilot plants of up to 1.7 MW_{th}, achieving CO_2 capture rates over 90% (Ströhle et al., 2020). Despite not achieving industrial application yet, they are gaining increasing attention thanks to their non-toxic technology, and the integration flexibility with existing combustion systems (Zhang et al., 2024).

One of the drawbacks of this technology is the gradual decline in the sorption capacity of CaO with each cycle of carbonation and calcination (Grasa & Abanades, 2006). To address this issue and maintain an efficient carbonation performance, a fraction of CaO must be purged, and fresh $CaCO_3$ must be introduced into the loop. Studies indicate that low purge rates of CaO help minimize operational costs of the CaL system, although this necessitates a greater amount of sorbent to be circulating within the loop (Romeo et al., 2009). Another feature of CaL technology is the necessity of generating pure oxygen for the oxy-combustion of $CaCO_3$ in the calciner. As a result, CO_2 and water are the only gaseous products of the calcination, which facilitates efficient CO_2 capture. A basic process flowsheet of a CaL configuration is shown in Fig. 2.

Numerous studies have analysed the possibilities of integrating CaL technology into different carbon-intensive industries, such as steelmaking (Perpiñán et al., 2023), glassmaking (Barón et al., 2023), the cement industry (Liu et al., 2023), and waste-to-energy plants (Haaf et al., 2020). The use of $CaCO_3$ to form calcium-aluminate slags in the Pedersen process makes calcium looping a very interesting alternative to minimize CO_2 emissions and developing a self-sufficient plant, using purged CaO for the production of slags and captured CO_2 as feedstock for the precipitation of aluminium hydroxide.

1.3. Objectives

Considering all previous studies mentioned above and the current state of the art, this work aims to establish, for the first time, the global material and energy balances of the Pedersen process for different bauxites throughout process simulation, with the goal of evaluating the potential advantages of this technology over the conventional production of alumina via the Bayer process. The co-production of smelter-grade alumina and pig iron from bauxite is evaluated based on thermodynamics and data from published experimental studies. For that purpose, three different compositions of bauxite ore are considered, and material and energy performances are studied in each case.

Additionally, this work introduces as a novel contribution the integration of a calcium-looping plant into a prospective Pedersen plant. Under the same simulation environment, the aim is to analyse the energy penalty for providing a source of CO_2 and CaO necessary for the process and avoiding fossil fuel-derived CO_2 emissions. This penalty is quantified for each kind of bauxite ore, and potential advantages and

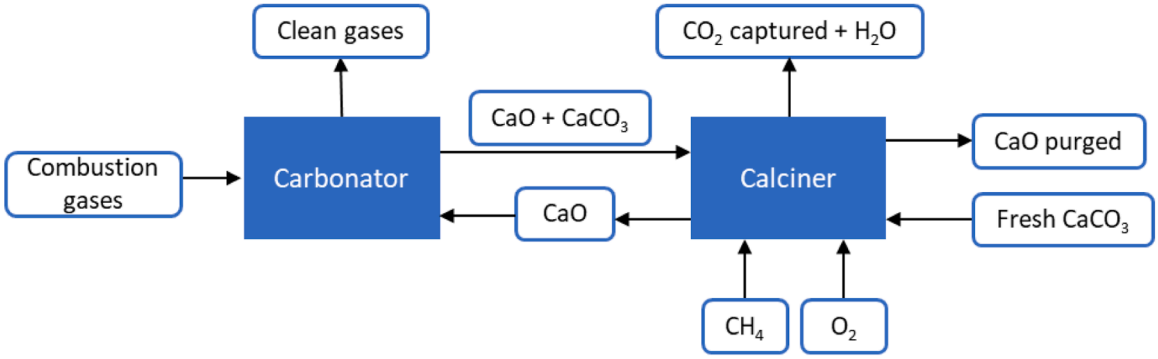

Fig. 2. Simplified flowsheet of a calcium looping plant.

disadvantages of the integration are further discussed. Various operating parameters of the calcium-looping system, such as the CaO purge rate and the circulation ratio, are also examined to determine the optimal configuration.

2. Material and methods

Three different scenarios of a Pedersen process plant were developed using Aspen Plus V12.1 software. The plants were sized for a capacity to treat nearly 1.5 million tonnes of bauxite per year and three different bauxites with diverse Al/Fe ratios were included in the analysis. The compositions of each bauxite employed in the study are shown in Table 1. Three compositions of bauxite with different aluminium content were proposed with the aim of evaluating low-grade and high-grade bauxites, adapting their composition to match with the average values of aluminium content found in bauxite (Hudson et al., 2012). To ensure the similarity with industrial bauxite, the selected compositions were chosen within ranges reported for metallurgical-grade bauxites (>45 % weight Al_2O_3), meeting standard industrial specifications (Bogatyrev & Zhukov, 2009). Compositions ranges typical of major global deposits, such as the Mediterranean bauxites (Al_2O_3 ~45–55 %, SiO_2 ~2–10 %, Fe_2O_3 ~15–23 %) and African ores (with Al_2O_3 approximately 44–61 %, Fe_2O_3 1.6–34 %, SiO_2 0.4–10.8 %), were used to guide the selection (Zainudeen et al., 2023, Banerjee et al., 2023), thereby ensuring that the simulation cases are representative of industrial feedstocks. Following this, three additional scenarios of a CaL system were also developed for each bauxite to treat the corresponding combustion gases of the plants and different energy and material optimizations were implemented for each case.

2.1. Pedersen process plant

The Pedersen plant models comprehend the production of pig iron, grey mud and alumina from bauxite, using natural gas as the fuel to obtain the required thermal energy. Natural gas combustion is selected as the thermal energy source given the majority of European alumina refineries that employ this fuel (European Aluminium Association). The composition of natural gas is assumed as 100% methane to easy the modelling of the reactions. Limestone ($CaCO_3$) is used along with bauxite for its proper leaching in Na_2CO_3 solution. Carbon anodes are also used to produce pig iron, and a pure stream of CO_2 is assumed to precipitate aluminium hydroxide. A detailed flowsheet of the plant, with its designed system of heat exchangers, is shown in Fig. 3.

Firstly, bauxite particle size is mildly reduced in a crusher to make it suitable for industrial processing. The modelling of the particle size reduction is carried out assuming a normal distribution of the particle size of the initial ore of 5 mm and a standard deviation of 1 mm. The electricity demand of the milling is estimated following Bond's Law of size reduction (Bond, 1961) considering the maximum particle size of the ore as 750 μm (Königsberger, 2008).

After the grinding, bauxite is heated together with limestone at 900°C to dehydrate the rock before the smelting-reduction step. This stage is modelled using an RGibbs reactor in Aspen Plus, which assumes thermodynamic equilibrium based on Gibbs free energy minimization. This assumption is justified due to the high operating temperature and the long residence time expected in real applications. In practice, this thermal treatment could be carried out in a rotary kiln, which is widely used in cement and lime industries for solid–gas contact at high temperatures (Kaczyńska et al., 2021). Bubbling fluidized bed (BFB) reactors, although not commonly used in current industrial lime or cement production (JRC Reference Reports 2013), have also been proposed for integrating indirectly heated CaL systems into such processes (Hanak et al., 2015). However, BFBs face upscaling challenges compared to circulating fluidized beds (CFBs), which offer better gas-solid contact and scalability. Accordingly, most CaL studies favour the use of CFBs or entrained-flow reactors for both the carbonator and the calciner stages.

A 12/7 molar ratio of Ca/Al is assumed to estimate the amount of limestone needed in the dehydration of bauxite, considering that $12CaO{\cdot}7Al_2O_3$ slag formation is preferred for the leaching stage (Ma et al., 2022). The combustion of natural gas is also modelled within the same RGibbs reactor, under the assumption of complete combustion with excess air, as in practice, this reaction would occur in an integrated combustion chamber within the calcination system (Kaczyńska et al., 2021). Thus, the chemical reactions occurring at this stage are shown in Reactions **(1)-(3)**, in which the thermodynamic equilibriums are calculated assuming no kinetics restrictions.

$$CH_4\ (g) + 2O_2\ (g) \rightarrow 2H_2O\ (g) + CO_2\ (g)\ \Delta H_r^0 = \text{-802.0 MJ/mol } CH_4 \quad (1)$$

$$2Al(OH)_3\ (s) \rightarrow Al_2O_3\ (s) + 3H_2O\ (g)\ \Delta H_r^0 = 185.2\ \text{kJ/mol } CH_4 \quad (2)$$

$$CaCO_3\ (s) \rightarrow CaO\ (s) + CO_2\ (g)\ \Delta H_r^0 = 178.0\ \text{kJ/mol CaO} \quad (3)$$

As shown in Fig. 3, residual heat from the flue gases released from Reactions **(1)-(3)** is exploited to preheat initial bauxite and limestone. Solids, otherwise, are sent to an electric arc furnace, in which electricity

Table 1
Different compositions (in mass fractions) of bauxite used in the study (Hudson et al., 2012, Zainudeen et al., 2023).

Bauxite	$Al(OH)_3$ (% wt)	Fe_2O_3 (% wt)	SiO_2 (% wt)	TiO_2 (% wt)
Baux5.4 (Ratio Al/Fe=5.4)	87.8	8.0	2.7	1.5
Baux2.5 (Ratio Al/Fe=2.5)	80.1	15.7	2.7	1.5
Baux1.5 (Ratio Al/Fe=1.5)	72.4	23.4	2.7	1.5

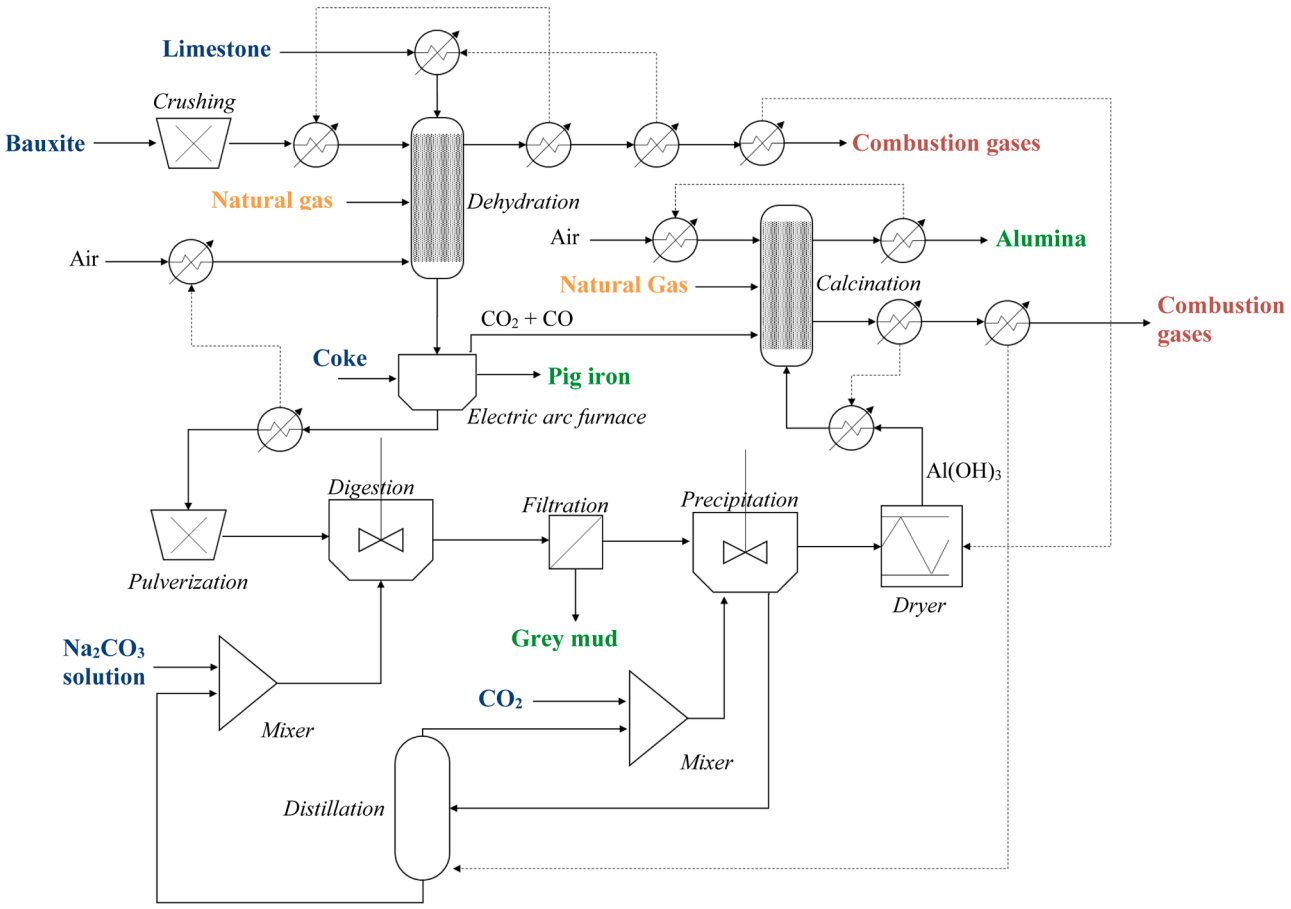

Fig. 3. Detailed flowsheet of the Pedersen process plant simulation.

and carbon anodes (modelled as 100% carbon) are consumed to smelt the iron content of bauxite. Silicon content is also partially reduced at 1500°C (Safarian & Kolbeinsen, 2016). Formation of mayenite phase ($12CaO{\cdot}7Al_2O_3$) is also assumed to occur primarily (Georgala et al., 2023). The reactions that happen in this stage are shown in Reactions **(4)-(6)**. Due to the lack of data regarding the kinetics of this stage, the high-temperature smelting step is simulated using RStoic reactors, with conversion values obtained from experimental data (Keplinger et al., 2018) and constrained so as not to exceed the thermodynamic equilibrium limits. Although kinetics are not modelled explicitly, this assumption provides a reasonable approximation for mass and energy balances, as they are based on the conversion rates observed in the experiments from literature. The industrial reactor corresponding to this stage is an Electric Arc Furnace, which is widely used for reduction reactions and alloy production at similar temperatures (Conejo, 2024).

$$Fe_2O_3\ (s) + 2C\ (s) \rightarrow 2Fe\ (s) + CO_2\ (g) + CO\ (g) \quad (4)$$

$$3SiO_2\ (s) + 4C\ (s) \rightarrow 3Si\ (s) + 2CO_2\ (g) + 2CO\ (g) \quad (5)$$

$$12CaO\ (s) + 7Al_2O_3\ (s) \rightarrow 12CaO{\cdot}7Al_2O_3\ (s) \quad (6)$$

The smelted iron, containing silicon and traces of carbon, is cast on-site for its commercialization. On the other hand, the mayenite solid phase is put through a pulveriser to reduce its particle size before digestion on Na_2CO_3 solution. The cooling down of the solid phase must be carried out at a controlled rate to enable the formation of the desired slag phase (Azof et al., 2018). A small fraction of heat residues from the slag is exploited to preheat the air necessary during the dehydration of bauxite. The mixture of CO and CO_2 released during the reduction of iron and silicon is trapped and sent to the aluminium hydroxide calciner to maximize the energy recovery. After pulverization of mayenite, the main reaction assumed to occur at the digestion stage is shown in Reaction **(7)**.

$$12CaO{\cdot}7Al_2O_3\ (s) + 12Na_2CO_3\ (s) + 33H_2O\ (l) \rightarrow 12CaCO_3\ (s) + 14NaAl(OH)_4\ (aq) + 10NaOH\ (aq) \quad (7)$$

The digestion step is simulated using an RStoic reactor, with reaction extents based on literature experiments (Georgala et al., 2023). This was selected as the most appropriate assumption to carry out the modelling, as the process operates at relatively low temperature (around 100°C) and is limited by solubility and reaction kinetics. In a real plant, digestion would likely be carried out in stirred tank reactors (STRs) operating in batch or semi-batch mode, as commonly found in hydrometallurgical and Bayer-type leaching processes (Bánvölgyi & Haneman, 2022).

After the leaching unit, grey mud sludge is filtrated and separated for its disposal or commercialization, and aqueous $NaAl(OH)_4$ is carried to a precipitator where an excess flow of pure CO_2 is fed. The input of CO_2 is estimated as the amount of CO_2 necessary to supersaturate the solution, ensuring the complete precipitation of aluminium hydroxide ($Al(OH)_3$). The precipitation reactions are again modelled using RStoic reactors, where conversion is defined by stoichiometry and the assumed CO_2 input. These reactions are simulated under equilibrium assumptions, although the kinetics of nucleation and growth govern the product formation. Thus, the yield of this stage could be overestimated, depending on the size and time residence of the precipitation stage in real operation. Industrially, this stage would take place in agitated precipitation tanks, similar to those used in Bayer process operations (Bánvölgyi & Haneman, 2022). Both reactions of $Al(OH)_3$ precipitation and Na_2CO_3 regeneration that take place at this stage are shown in

Reaction **(8)** and Reaction **(9)**.

$$2NaAl(OH)_4\ (aq) + CO_2\ (g) \rightarrow Na_2CO_3\ (s) + 2Al(OH)_3\ (s) + H_2O\ (l) \quad (8)$$

$$2NaOH\ (aq) + CO_2\ (g) \rightarrow Na_2CO_3\ (s) + H_2O\ (l) \quad (9)$$

$Al(OH)_3$ is filtrated and washed, and residual heat from flue gases leaving the bauxite dehydration is used to dry $Al(OH)_3$ before entering the calciner to produce smelter grade alumina. The remaining liquid after the digestion contains a Na_2CO_3 aqueous solution saturated with CO_2. Hence, a distillation column is proposed to extract CO_2 from the solution and recycle it back to the precipitator. Similarly, Na_2CO_3 concentration is adjusted with fresh solution and reused in the digestion unit.

Finally, dry $Al(OH)_3$ is calcined at 1100°C, for which natural gas is used again as fuel. The reactions that take place are the same as Reaction **(1)** and Reaction **(2)**, obtaining smelter grade alumina as the product of the process. Alumina is dried with pre-combusted air. Likewise, thermal energy from flue gases of this stage are exploited to preheat the hydroxides and at the distillation unit of the CO_2-H_2O phase.

The main technical assumptions considered for the global implementation of the Pedersen process plant are listed on Table 2. The results of the three models, including the mass flows, compositions and temperatures of each stream, are also detailed in Appendix A.

Table 2
Technical assumptions and operating conditions considered for the implementation of the Pedersen plant.

Unit Process	Parameter	Value
Crushing	Initial particle size	D50= 5 mm; σ=1 mm
	Required particle size	<750 μm
	Bond Work Index	11 kWh/tonne (Bond, 1961)
	Mechanical Efficiency	0.85
Bauxite Dehydration	Temperature	900°C (Ma et al., 2022)
	Reaction (1) extent	Gibbs energy minimization
	Reaction (2) extent	Gibbs energy minimization
	Reaction (3) extent	Gibbs energy minimization
	Air input	5% stoichiometric excess
	$CaCO_3/Al_2O_3$ molar ratio	12/7 (Ma et al., 2022)
Electric Arc Furnace	Temperature	1550°C (Keplinger et al., 2018)
	Electrical efficiency	0.72 (Keplinger et al., 2018)
	Reaction (4) extent	99.5% (Azof et al., 2018)
	Reaction (5) extent	10.6% (Safarian and Kolbeinsen, 2016)
	Reaction (6) extent	98.0% (Ma et al., 2022)
	Coke anode consumption	Stoichiometric
Pulverization	Required particle size	<160 μm
	Bond Work Index	11 kWh/tonne (Bond, 1961)
	Mechanical Efficiency	0.85
Digestion	Temperature	70°C
	Reaction (7) extent	94% (Georgala et al., 2023)
	Na_2CO_3 concentration	75 g/L (Georgala et al., 2023)
	Solid/Liquid mass ratio	0.08 (Georgala et al., 2023)
Precipitation	Temperature	50°C (Sidrak, 2001)
	CO_2 consumption	Until reaching CO_2 saturation in liq. phase
	Reaction (8) extent	Gibbs energy minimization
	Reaction (9) extent	Gibbs energy minimization
Distillation	Number of stages	6
	Top temperature	25°C
	Bottom temperature	90°C
	Feed stage	4
Calcination	Temperature	1100°C (Sidrak, 2001)
	Air input	5% stoichiometric excess
	Reactions extent	Gibbs energy minimization
Heat Exchangers System	Minimum temperature interval	30°C

2.2. Integration of the calcium-looping plant

CaL technology is proposed to capture the CO_2 contained in the flue gases that leave the bauxite dehydration unit and the calcination of aluminium hydroxide. The implementation of the CaL models were also performed using Aspen Plus V12.1 software, following the same configuration that was shown in Fig. 2. Many scientific studies have already developed and analysed CaL systems using Aspen Plus software, focusing on carbon capture efficiency, energy penalties, and process optimization. The methodology usually is based on the use of the built-in fluidized bed models from Aspen Plus (Hejazi & Grace, 2020), the use of stoichiometric reactors (RStoic) (Jiang et al., 2024) or the use of Gibbs free energy minimization reactors (RGibbs) (He et al., 2025).

In this work, carbonation is simulated with an RStoic reactor using a well-validated deactivation model, neglecting explicit treatment of kinetic limitations, diffusional resistance, and non-ideal solid–gas contact. The models developed in this work consisted mainly of the simulation of a carbonation reactor (in which CO_2 contained in the gases reacts with CaO to produce $CaCO_3$) using an RStoic unit, and an oxy-fuel calciner (in which CO_2 is released from $CaCO_3$) using an RGibbs unit. The RStoic model allows to fix the value of the conversion of a pre-defined set of chemical reactions. In contrast, the Gibbs reactor allows to estimate the thermodynamic equilibrium of a mixture of components by minimizing the Gibbs energy of the system. These units are useful to estimate the thermal energy demands and the thermodynamic limits of a system. However, since the model does not account for kinetic limitations such as surface reaction resistance, intraparticle diffusion, and imperfect gas–solid contact, the simulated carbonation conversion could result higher than what would be observed in practical fluidized bed reactors.

For a more realistic representation, several published models incorporate solid–gas kinetic and diffusion effects—predominantly based on two-zone fluidization models of Kunii–Levenspiel (K–L), combined with shrinking-core or random-pore reaction kinetics. For example, Sattari et al. (Sattari et al., 2021) proposed a fluidized bed carbonator model using Kunii–Levenspiel theory that captures bed hydrodynamics, superficial gas velocity, solids fractions in bubble/emulsion regions, and sorbent decay over cycles; predictions aligned with pilot-scale experiments. Similarly, Abanades et al. (Abanades et al., 2004) employed two-zone K–L mass balances coupled with kinetic and gas-transfer limitations to predict real capture efficiencies in circulating fluidized beds. Yao et al. (Yao et al., 2017) also developed a two-phase model combining CSTR (emulsion) and PFR (bubble) zones incorporating a random-pore kinetic model to account for surface and diffusion-controlled carbonation rates under elevated pressures.

Hence, our current model, which neglects these kinetic and diffusion resistances, could result slightly optimistic in terms of predicted carbonation conversion and CO_2 capture efficiency, compared to models that account for limited sorbent accessibility, transport resistances, or imperfect mixing. Nevertheless, this simplified approach serves to bound the thermodynamic potential of the system. To further analyse the economic implications of the system, the modelling of a fluidised bed reactor should be implemented, in order to account for additional non-ideal conditions (such as mass transfer limitations) while allowing the real sizing of the equipment (Porrazzo et al., 2014). Implementation of such more advanced models (e.g. Kunii–Levenspiel two-zone K–L model plus random-pore kinetics or shrinking-core kinetics) remains subject for future work.

The conversion of CaO in the carbonator was calculated according to the methodology indicated in previous works (Sáez-Guinoa et al., 2024), which is based on the conversion of one single particle of CaO and the estimation of the average number of cycles that CaO suffers, as proposed initially by Grasa and Abanades (Grasa and Abanades, 2006). This estimation method consists of a series of semi-empirical equations, which were developed by carrying out laboratory-scale experiments on a thermogravimetric analyzer designed for long multicycle carbonation-calcination tests. Results with different type of limestones

indicated that the capture capacity of the sorbent suffers a strong decay during the first 20 carbonation-calcination cycles, but then it tends to stabilize, showing a residual activity of 0.075-0.08 after 500 cycles (Grasa and Abanades, 2006). This semi-empirical method has been widely used and adapted by practitioners thanks to its accuracy and relatively low level of complexity (Amorim et al., 2025, Shafiabadi et al., 2025, Hejazi & Montagnaro, 2024, Romano, 2012, Greco-Coppi et al., 2025). More recently, this method was successfully validated in pilot tests in a 300kW$_{th}$ plant, fitting the model with reasonable accuracy with the empirical degrees of carbonation (Greco-Coppi et al., 2025).

The conversion of CaO is very influenced by the physical properties of the sorbent used. Hence, the characteristics of the limestone selected for this study were retrieved from Pascual et al. (Pascual et al., 2021). The study of a different sorbent or an alternative calculation method of the sorbent deactivation remain as a future task to check its influence in overall results.

The modelling of the carbonation was developed by considering the number of cycles of carbonation-calcination (N) of a limestone ($CaCO_3$) particle as a reference. As the sorption capacity of the solid decays after each cycle, a typical limestone sorption capacity was used in the calculations (Grasa & Abanades, 2006). Equation 1 shows the conversion of one particle of CaO (X_N) in the carbonator as a function of its number of cycles N. In this equation, k is the conversion decay constant, set as 0.52, and X_r is the residual activity of CaO particles after an infinite number of cycles, which was assumed as 0.075 (Grasa & Abanades, 2006) for the limestone selected in this work.

$$\mathbf{X_N} = \frac{1}{\frac{1}{1-\mathbf{X_r}} + \mathbf{k}\cdot\mathbf{N}} + \mathbf{X_r} \tag{10}$$

Thus, the average conversion achieved by the solid CaO particles (X_{ave}) is calculated as the product of their distribution of the number of cycles (r_N) and the conversion of each particle, X_N. The calculation of the average conversion (X_{ave}) of the CaO particles is shown in Equation 2, in which r_N represents the percentage number of CaO particles that have passed through a certain number of cycles N.

$$\mathbf{X_{ave}} = \sum_{\boldsymbol{N}=1}^{\boldsymbol{N}=\infty} \boldsymbol{r_N}\cdot\mathbf{X_N} \tag{11}$$

To calculate the variable r_N, the molar flowrates of CaO entering the carbonator (F_{CaO}) and $CaCO_3$ entering the oxy-calciner (F_0) were used, as shown in Equation 3.

$$\mathrm{r_N} = \frac{\frac{\mathrm{F_0}}{\mathrm{F_{CaO}}}}{\left(1+\frac{\mathrm{F_0}}{\mathrm{F_{CaO}}}\right)^{\mathrm{N}}} \tag{12}$$

Two key parameters need to be defined to estimate the conversion of CaO at the carbonator, and hence, the efficiency of the CO_2 capture system: the molar ratio of CaO/CO_2 entering the carbonator, known as the carbonation ratio (R), and the percentage of CaO that is replaced by fresh $CaCO_3$ after the oxy-fuel calcination, known as the purge ratio (f_p) (Rodriguez et al., 2008). High carbonation and purge ratios increase the efficiency of the carbon capture. To minimize economic costs, configurations with low purge ratios and high carbonation ratios are usually preferred (Romeo et al., 2009), reducing the purchase cost of fresh limestone. However, this study proposes to explore integrating a CaL system in a process with an existing demand of fresh $CaCO_3$. Therefore, the integration of CaL configuration into the Pedersen plant can be based on diverse linkages, aside from the flue gases entering the carbonation unit. Purged CaO leaving the CaL system can be fed into the bauxite dehydration unit by substituting initial $CaCO_3$. Thereby, CO_2 released from the decomposition of $CaCO_3$ in that unit decreases, obtaining a synergistic effect on the energy consumption needed to capture the CO_2 of the whole system.

A temperature of 650°C was fixed in the carbonator reaction to allow for a suitable CaO conversion. Thus, the carbonator was assumed to be cooled down to maintain its temperature, as it is necessary due to the exothermicity of the reaction. Similarly, thermal heat of the material streams (mainly the CaO sorbent and the flue gases from the Pedersen process) was recovered to decrease their temperature. The recovered heat was then exploited in different stages of the process, such as the distillation and the drying of the Pedersen plant. Hence, the released heat from the carbonation reaction serves to adjust the temperature of the input flows, making the net duty of the carbonation equal to zero. In contrast, the feed of natural gas (and a 5% stoichiometric excess of oxygen) in the oxy-fuel calciner was calculated to achieve a temperature of 900°C for the reactants. Additionally, A 33% mass fraction of CO_2 released during the oxy-fuel combustion was recirculated back to the oxy-calciner in order to simulate the conditions of the oxy-fuel combustion to real fluidised bed reactors (Guo et al., 2024). Thus, the recirculation of CO_2 eases the temperature distribution and ensures a correct fluidization velocity at the bed reactor, while diluting oxygen to control the temperature of the combustion (Martínez et al., 2012). Main operational conditions that were assumed for the CaL implementation and integration are gathered in Table 3.

Different carbonation and purge ratios were analysed to find the optimal integration based on the particularities of the Pedersen process. Low and mid-purge ratios were evaluated, whereas the carbonation ratios were the result of fixing the maximum amount of CO_2 emitted as 2% of the initial CO_2 emissions of the Pedersen simulation. A third additional case was implemented, in which the purge ratios were maximized in order to cover the complete demand for calcium oxide from the Pedersen plant for each of the bauxites considered in the study. The 2% limit on the CO_2 maximum emissions was set equally for all the cases under study, in order to stablish fair comparisons between the different case studies. A 98% reduction of the CO_2 emissions was set as an achievable upper value in integrated systems (Romeo et al., 2011), considering also the expected CO_2 avoidance thanks to the recycling of spent CaO in the bauxite dehydration unit. The values of the key parameters (purge and carbonation ratios) used for each case study are gathered in Table 4, along with the obtained values for the efficiency of the carbonation (E_{carb}) and the overall carbon capture efficiency (E_{cc}). E_{carb} is an indicator limited to the performance of the carbonation unit, and it is calculated as the percentage of CO_2 that is absorbed in the carbonation unit with respect to the total amount of CO_2 entering the carbonator. In contrast, E_{cc} provides an indicator for the entire CaL system, representing the fraction of CO_2 released (captured) in the oxy-fuel calciner with respect to the total amount of CO_2 generated in the process.

The detailed flowsheet of the integration of both systems is shown in Fig. 4 for the cases in which purged CaO from the oxy-fuel calciner does not cover the demand for calcium oxide at the bauxite dehydration unit. In these cases, only the fraction of fresh limestone that enters the dehydration unit is preheated using CO_2 leaving the oxy-fuel calciner at 900°C, whereas spent CaO sorbent from the CaL unit is directly fed into the dehydration unit at 650°C to minimize the energy consumption. The heat exchangers system suffers several modifications, as the thermal energy residues available in the dehydration unit decreased remarkably

Table 3
Operating conditions of CaL system.

Variable	Units	Value
Carbonator temperature	°C	650 (Pascual et al., 2021)
Oxy-fuel calcination temperature	°C	900 (Pascual et al., 2021)
Oxygen feed	-	5% stoichiometric excess (Barón et al., 2023)
Electricity consumption for oxygen generation	kWh/tonne O_2	225 (Strojny et al., 2023)
Electricity consumption for CO_2 compression	kWh/tonne CO_2	90 (Jackson & Brodal, 2019)
CO_2 recirculation	%wt	33 (Pascual et al., 2021)

Table 4
Values of key parameters studied for the CaL integration.

Variable	Baux5.4			Baux2.5			Baux1.5		
Purge ratio	Low	Mid	Max	Low	Mid	Max	Low	Mid	Max
Carbonation ratio (-)	5.05	1.84	1.55	5.04	1.84	1.60	5.05	1.85	1.68
Purge ratio (%)	2.6	33.3	55.2	2.6	33.3	50.0	2.6	33.3	44.2
E_{carb} (%)	94.79	94.12	92.24	94.57	94.01	92.88	94.21	93.87	92.79
E_{cc} (%)	97.25	96.88	96.33	97.27	96.72	96.45	97.26	96.92	96.79

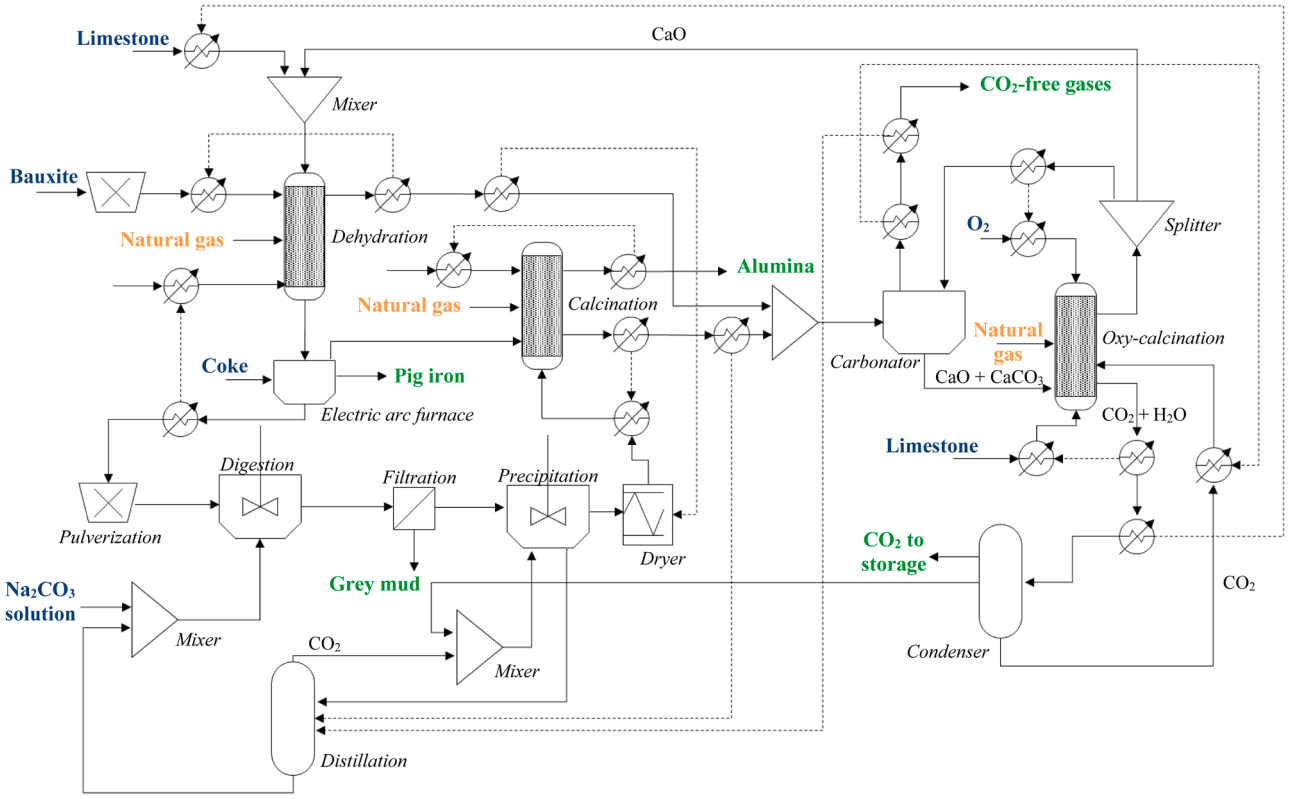

Fig. 4. Detailed flowsheet of the CaL and Pedersen plant integration for low and mid purge ratios.

thanks to the recirculation of spent CaO sorbent. Additionally, the combustion gases from the Pedersen plant are now only partially cooled down below 650°C to meet the required temperature of the carbonator. Therefore, the new heat residues available from the clean gases without CO_2 leaving the carbonation unit of the CaL plant need to be exploited to separate CO_2 and Na_2CO_3 solution at the distillation unit, which was carried out solely with the thermal energy from the combustion gases in the previous single Pedersen configurations.

The resulting layout of the integration of a CaL system that purges enough CaO to meet completely the demand of the bauxite dehydration unit is displayed in Fig. 5. In these cases, no heat exchanger is needed for the $CaCO_3$ entering the dehydratrion unit. Therefore, the CO_2 stream leaving the oxy-fuel calciner at 900°C is exploited to preheat the flow of fresh limestone entering the same unit, as the energy requirements of this mass flow have increased since the entire demand for $CaCO_3$ enters the oxy-fuel calciner. In contrast, clean gases leaving the carbonator are now used to preheat bauxite as much as possible. No fresh limestone is needed at the dehydration unit since calcined CaO reaches the demand for the formation of $12CaO{\cdot}7Al_2O_3$.

Finally, in both integrations, CO_2 leaving the oxy-fuel calcination is separated from water by water condensation. CO_2 stream is then used as feedstock at the $Al(OH)_3$ precipitation stage, minimizing the amount of CO_2 to be compressed and sent to storage or other purposes. The results of the models of the three purge ratios evaluated for each type of bauxite, including the mass flows, compositions and temperatures of each stream, can be found in Appendix B.

3. Results and discussion

3.1. Single Pedersen plant: materials and energy performance

Results regarding raw materials consumption and outputs production from Pedersen plant simulation are summarized in Table 5 for each of the three bauxites described in this work. The results show that the demand for $CaCO_3$ in the Pedersen process increases proportionally to the alumina content of the ore. So does the amount of CO_2 directly emitted during the process because of the increased energy demand to produce alumina and the higher amount of CO_2 released from using $CaCO_3$. Although production volumes of alumina depend strongly on bauxite initial composition (Ruys, 2019), the results of the Pedersen process show the potential valorisation of iron content, minimizing bauxite residue production. The Bayer process is estimated to produce around 0.4-0.7 tonnes of bauxite residue per tonne of bauxite (Evans, 2016), whereas the Pedersen process avoids those residues, presenting a production volume of 0.427-0.518 tonnes of alumina and 0.059-0.172 tonnes of pig iron per tonne of bauxite treated.

Compositions of the three main outputs of the process are also shown in Table 6. No relevant differences were found among the different

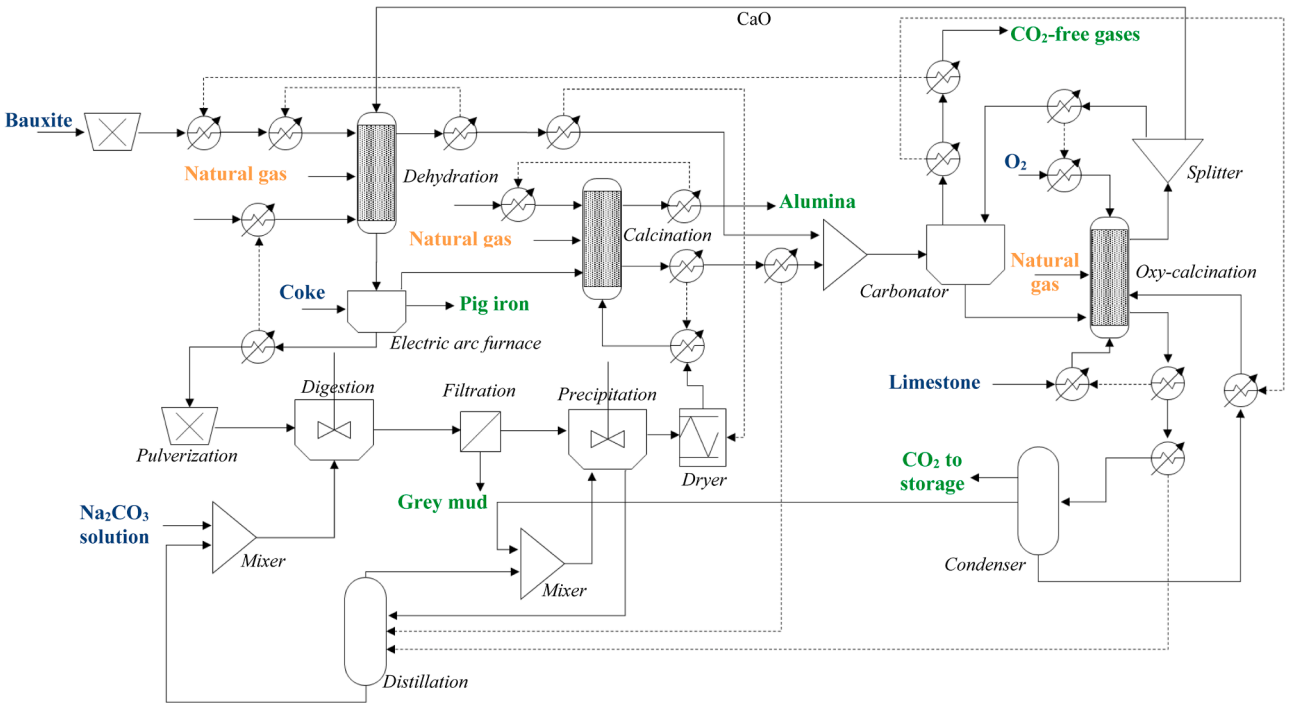

Fig. 5. Detailed flowsheet of the CaL and Pedersen plant integration for maximum purge ratios.

Table 5
Mass flowrates of inputs and outputs per tonne of processed bauxite.

Mass flows (tonnes/tonne of bauxite)	Baux5.4	Baux2.5	Baux1.5
Inputs			
Bauxite	1.000	1.000	1.000
Natural Gas	0.119	0.105	0.092
$CaCO_3$	0.966	0.881	0.796
Coke	0.015	0.030	0.044
Na_2CO_3	0.205	0.180	0.160
Water	0.840	0.756	0.691
CO_2	0.392	0.358	0.325
Outputs			
Alumina	0.518	0.473	0.427
Pig Iron	0.059	0.116	0.172
Grey Mud	1.489	1.349	1.218
CO_2 (emitted to air)	0.807	0.771	0.741

Table 6
Weight compositions of three main outputs from Pedersen process.

Compounds (mass fractions)	Baux5.4	Baux2.5	Baux1.5
Alumina			
Al_2O_3	0.999	0.998	0.998
Na_2O	<0.001	<0.001	<0.001
SiO_2	<0.001	<0.001	<0.001
Pig Iron			
Fe	0.939	0.943	0.945
C	0.040	0.045	0.048
Si	0.021	0.012	0.007
Grey Mud			
$CaCO_3$	0.621	0.611	0.599
Water	0.204	0.205	0.205
Na_2CO_3	0.099	0.102	0.105
$12CaO{\cdot}7Al_2O_3$	0.046	0.045	0.044
SiO_2	0.016	0.017	0.020
TiO_2	0.009	0.008	0.008

cases. Slight traces of sodium oxide and silicon dioxide could be found in alumina, according to the assumptions made during the study. However, these traces do not jeopardize the quality of alumina, as smelter grade alumina usually requires a purity of more than 98.5% (Yang et al., 2020), and the results found in the study show a purity of 99.8%. Similarly, carbon content in pig iron remains around 4-5%wt, making it suitable for its use in the steelmaking industry (Perpiñán et al., 2023). Furthermore, as indicated by previous studies analysing the composition of grey mud (Vafeias et al., 2018), the composition of grey mud obtained in the study shows no iron content and lower alkalinity than bauxite residue, making it a safer option for long-term disposal and being a promising candidate for valorisation to be used as a raw material in the cement industry or as a soil additive (Azof et al., 2020).

Regarding energy demand, the net energy consumption of the different units of the models are shown in Table 7. Results show that energy consumption is around 13.28-14.25 GJ per tonne of alumina produced. These figures are slightly lower than the actual estimations of the former industrial Pedersen plant, which needed around 14.40 GJ to produce 1 tonne of alumina (Miller & Irgens, 2013). The difference can be explained because of the calcination temperature of the industrial plant (1250°C), which was set higher than strictly required. Thus, flue gas with an adequate concentration of CO_2 was obtained to be used at the precipitation stage (Miller & Irgens, 2013). Nonetheless, the results

Table 7
Results of energy consumptions at the diverse stages of Pedersen process.

	Baux5.4	Baux2.5	Baux1.5
Thermal Energy (GJ/tonne of Al_2O_3 produced)			
Bauxite Dehydration	7.754	7.965	8.055
Digestion	-	-	-
Precipitation	-	-	-
Distillation*	-	-	-
Calcination	4.354	3.702	3.307
Electrical Energy (kWh/tonne Al_2O_3 produced)			
Crushing	6.387	6.938	7.501
Electric Arc Furnace	304.173	518.894	779.440
Pulverization	15.013	15.013	15.013
Thermal Energy Consumption (GJ/tonne Al_2O_3)	12.108	11.667	11.362
Electricity Consumption (kWh/tonne Al_2O_3)	325.573	540.845	801.954
Total Energy (GJ/tonne Al_2O_3)	13.280	13.615	14.249

* Distillation requires 2690-2750 MJ/tonne, but energy requirement is recovered from residual heat, hence, no net consumption occurs.

of this work show that energy consumption surpasses, in all cases, the average consumption of the Bayer process, which is estimated at 10.22 GJ/tonne. The higher energy demand of the Pedersen process is expected because of the addition of $CaCO_3$ throughout the process and the valorisation of the iron content of the ore. Considering that, on a world average, 1.22 tonnes of bauxite residue are generated per tonne of alumina, an estimation of the energy penalty for avoiding bauxite residue can be calculated as the subtraction of energy consumption from Pedersen plant minus average Bayer plants. Thus, it is obtained a specific primary energy cost of 2.51-3.30 GJ per tonne of bauxite residue avoided. The minor value range results similar to energy penalties for bauxite residue valorization, estimated at 2.40 GJ per tonne of bauxie residue valorized for cement industry (Di Mare & Ouellet-Plamondon, 2023). Nevertheless, economic analysis should confirm the viability of this route and the amelioration of this penalty.

Therefore, focusing on alumina production, it is shown that the Pedersen process could solve the bauxite residue generation but not alleviate the problematic high energy consumption that Bayer process plants present. However, some differences must be highlighted, such as the fact that alumina is not the only product of the Pedersen plant. Considering pig iron as a product with a similar marketability as alumina, net energy consumptions of the Pedersen process stand at 11.92, 10.93 and 10.15 GJ per tonne of products, for bauxites with Al/Fe ratios of 5.4, 2.5 and 1.5 respectively. Another alternative to present the results is considering the average energy demand of pig iron production, which is estimated at 17 GJ/tonne (Harvey, 2024). Therefore, a 'virtual' industry that achieves the production rates of alumina and pig iron shown in Table 5 for Baux5.4, Baux2.5 and Baux1.5 would require 12.16, 14.38 and 17.07 GJ per tonne of alumina respectively. Fig. 6 illustrates the energy performance as a function of the Al/Fe ratios of the ore, considering both references: the average energy consumption of a Bayer plant and the energy consumption that would be required for a 'virtual plant' to produce the same amounts of alumina and pig iron following conventional Bayer and blast furnace processes. Thus, as it is shown in Fig. 6, the Pedersen process can effectively compete with the Bayer process regarding energy requirements when using bauxites with a low Al/Fe content ratio, whereas the Bayer process performs better for bauxites with a higher alumina content.

Another significant difference is the type of energy requirements of both processes. Around 8.83-20.26% of the energy demand of the Pedersen process is electrical, whereas nearly 100% of the energy demand of the Bayer process is thermal energy. This difference is more remarkable as the Al/Fe ratio of the ore decreases, showing a good potential for minimization of CO_2 emissions in locations where renewable electricity is available. For illustration purposes, CO_2 emissions of the process were calculated for each of the three bauxites studied. To estimate the CO_2 emissions associated with electricity generation, an emission factor of 250 g of CO_2 per kWh_e was used, similar to the average CO_2 intensity of European markets (European Environment Agency 2023). Estimations of CO_2 emissions and their sources are displayed in Fig. 7. Based on these assumptions, results indicate that CO_2 emission intensity decreases as the Al/Fe ratio increases, with values between 1.76 tonnes of CO_2 (when bauxite Al/Fe ratio is 5.4) and 2.81 tonnes of CO_2 per tonne of products (for bauxites with 1.5 Al/Fe ratio). However, if CO_2 derived from electricity consumption is near zero thanks to the use of renewable electricity, CO_2 emissions result more similar, with estimations around 0.81-0.96 tonnes of CO_2 per tonne of products. By removing electricity-derived CO_2 emissions, and given that CO_2 feedstock nearly equals CO_2 coming from using $CaCO_3$, the combustion of natural gas becomes the leading emitter of CO_2. This contributor is close to constant, since it depends strongly on the amount of alumina that is calcined. Hence, the main difference in CO_2 emissions lies in the amount of coke used at the electric arc furnace. Therefore, it is shown that renewable electricity could become a relevant pathway for reducing environmental impacts due to alumina production. However, renewable electricity should be matched with other strategies to achieve a fully decarbonized industry.

3.2. Integration of calcium-looping plant to Pedersen plant

The efficiency of the proposed CaL system was fixed at 98%, understood as the percentage of CO_2 avoided over the initial CO_2 directly emitted with each of the three bauxite ores proposed. This efficiency is achievable thanks to the synergy effect between the CaO used in the Pedersen process and the CaO sorbent used in the CO_2 capture, which reduces drastically the CO_2 circulating in the system to be captured with respect to the single Pedersen process using $CaCO_3$ as feedstock. This synergistic effect can be also found in other industries that make use of calcium carbonate, such as the cement industry, in which CO_2 capture efficiencies of up to 95% have been achieved in 200 kWh_{th} pilot plant tests (Hornberger et al., 2017). The real efficiency obtained by the integrated layout, understood as the percentage of CO_2 captured over the amount of CO_2 entering the CaL system, is detailed in Table 4, showing values in the range of 92.2-94.8%. The obtained CO_2 capture extent falls within the range of the CO_2 capture efficiencies found in experimental pilot plants (Arias et al., 2024, Haaf et al., 2020), which usually vary between 85-95% depending on the residence time or the load of sorbent.

Consumption of primary raw materials (bauxite, Na_2CO_3, coke, water…) and production rates of alumina, pig iron and grey mud were not affected by the implementation of a CO_2 capture plant, as the chemistry of the process and the modelling assumptions shown in Table 2 were not modified. The overall demand for $CaCO_3$ was also unchanged, though its use as a sorbent to capture CO_2 entailed changes on the energy demand of the Pedersen plant. New disaggregated flowrates of $CaCO_3$ and natural gas of the integrated plants are gathered in Table 8, which shows also the amounts of CO_2 captured and CO_2 emitted

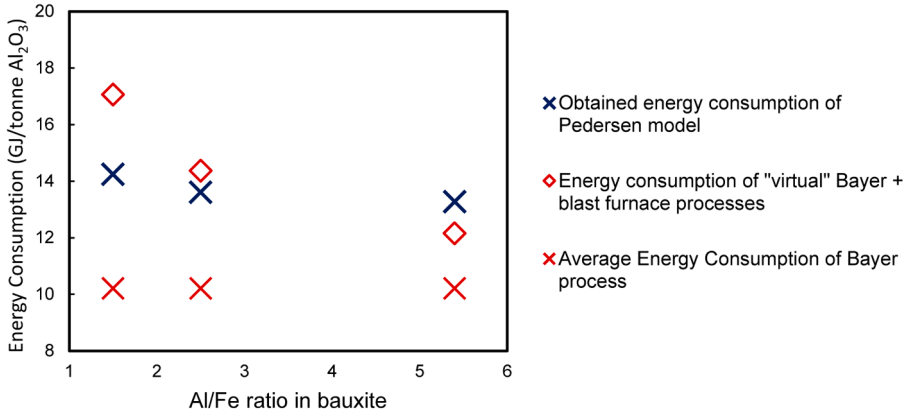

Fig. 6. Results of energy consumption as a function of Al/Fe ratio of the ore.

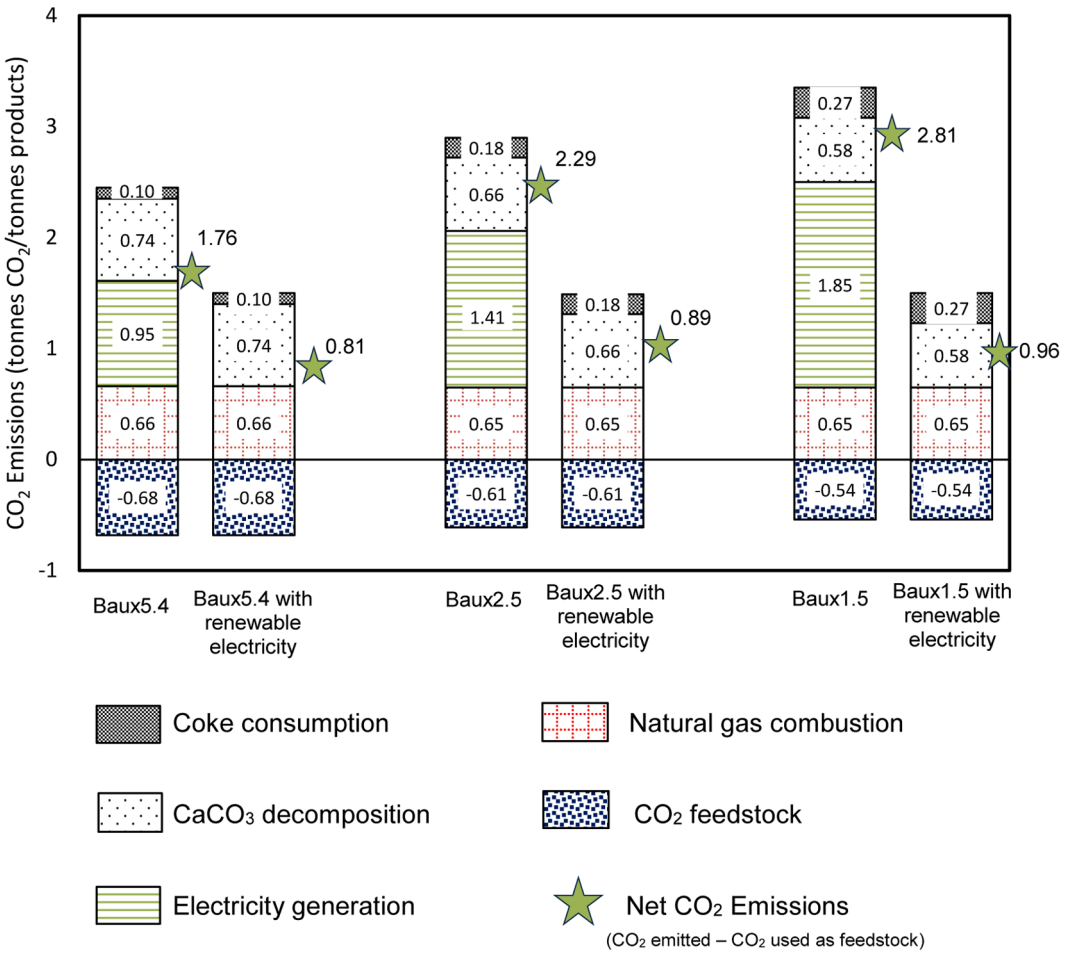

Fig. 7. Estimated CO_2 emissions per tonne of products. Disaggregation by source of CO_2.

Table 8
New mass flows of natural gas, limestone injection, CO_2 captured and CO_2 emitted for each case study of the CaL integration.

Variable (tonnes/tonne bauxite)	Baux5.4			Baux2.5			Baux1.5		
Purge ratio	Low	Mid	Max	Low	Mid	Max	Low	Mid	Max
$CaCO_3$ in bauxite dehydration unit	0.761	0.220	-	0.690	0.173	-	0.617	0.119	-
$CaCO_3$ in oxy-fuel calcination unit	0.205	0.746	0.966	0.191	0.708	0.881	0.179	0.677	0.796
Natural Gas in bauxite dehydration unit (GJ/tonne baux)	2.746	2.130	1.336	2.490	1.671	1.284	2.213	1.403	1.207
Natural Gas in hydroxide calcination unit (GJ/tonne baux)	1.397	1.414	1.449	1.345	1.351	1.353	1.237	1.249	1.251
Natural Gas in oxy-fuel calcination unit (GJ/tonne baux)	4.247	3.634	3.103	4.094	3.226	2.995	3.961	3.115	2.963
CO_2 Captured for storage	0.531	0.465	0.394	0.534	0.442	0.408	0.532	0.441	0.422
CO_2 directly emitted	0.015	0.015	0.015	0.015	0.015	0.015	0.015	0.014	0.014

to the atmosphere after the CaL integration. The proportion of fresh limestone injected at the bauxite dehydration unit varied as a function of the purge ratio at the oxy-fuel calcination of the CaL plant, also triggering a decrease in energy demands of the dehydration and the amount of CO_2 emitted at that unit. Hence, it is shown that higher ratios of CaO purge at the CaL plant induced significant reductions of energy demand both at the bauxite dehydration unit and the oxy-fuel calcination, drastically reducing the energy penalty of CO_2 capture. On the other hand, the energy demand of the hydroxide calcination unit remained unchanged with the diverse CaO purge ratios, since this energy input relies primarily on the amount of alumina produced. As a consequence of the overall energy decrease, the amount of CO_2 captured also decreases for higher CaO purge ratios, simplifying the downstream processing or storage of the carbon dioxide.

Table 9
Energy consumption and energy penalty of CaL integrations.

Variable	Baux5.4			Baux2.5			Baux1.5		
Purge ratio	Low	Mid	Max	Low	Mid	Max	Low	Mid	Max
Total Energy Consumption (GJ/tonne products)	16.99	14.14	12.73	16.46	13.24	12.18	15.85	12.50	11.98
Energy Penalty (%)	42.52	18.61	6.68	50.41	20.87	11.17	55.96	22.98	17.76
SPECCA (GJ/tonne CO_2 avoided)	7.38	3.26	1.10	8.25	3.48	1.89	8.57	3.56	2.79

Global energy consumptions of the different proposed integrations are gathered in Table 9, along with the energy penalty of CO_2 capture of each configuration. This energy penalty is calculated using two different methods: as a percentage of energy demand increase with respect to single Pedersen process, and as the specific primary energy consumption per tonne of CO_2 emissions avoided (SPECCA). The SPECCA values are calculated as shown in Equation 4, in which $Q_{th;CaL+Ped}$ and $Q_{th,Ped}$ are the thermal energy demands of the integrated CaL+Pedersen plant and the single Pedersen process respectively. As shown in the expression, the required electricity to generate oxygen for the oxy-fuel combustion (E_{O2}) and the electricity demand for CO_2 compression (E_{CO2}) are also accounted, multiplied by the primary energy factor of the average European electricity grid (PEF_{EU}), which converts the final electricity use into primary energy consumption, and equalled 1.9 in 2023 (European Commission 2022). The CO_2 avoided is estimated as the difference between the CO_2 emitted initially by the single Pedersen model ($m_{CO2;Ped}$) and the amount of CO_2 emitted after the CaL integration ($m_{CO2;CaL+Ped}$). The indirect emissions from electricity generation are also accounted ($m_{CO2;CaL;el}$), considering the average emission factor of the EU in 2023. For illustration purposes, estimations of total energy consumptions and SPECCA indices are plotted as a function of the CaO purge ratios in Fig. 8 and Fig. 9 respectively.

$$\text{SPECCA} = \frac{\dot{\mathbf{Q}}_{\text{th;CaL+Ped}} + (\dot{\mathbf{E}}_{\text{O}_2} + \dot{\mathbf{E}}_{\text{CO}_2}) \cdot \mathbf{PEF}_{EU} - \dot{\mathbf{Q}}_{\text{th;Ped}}}{\dot{\mathbf{m}}_{\text{CO}_2\text{;Ped}} - \dot{\mathbf{m}}_{\text{CO}_2\text{;CaL+Ped}} - \dot{\mathbf{m}}_{\text{CO}_2\text{;CaL;el}}} \quad (13)$$

Values of global energy consumptions show again that bauxites with low Al/Fe ratios are less energy-intensive per unit of product, whereas bauxites with a higher content of aluminium require more energy to be processed following the Pedersen route. However, implementing a CaL plant in different scenarios evidences two insights: the energy penalty of CO_2 capture becomes less for low Al/Fe ratios, and the use of high ratios of CaO purge entails a remarkable advantage.

By analysing bauxite with a 5.4 Al/Fe ratio, it is shown that a 2.6% purge ratio renders an energy penalty of 42.52% of the initial energy consumption of the single Pedersen plant, and a SPECCA value of 7.38 GJ per tonne of CO_2 avoided. While achieving the same efficiency of CO_2 capture (98% of initial CO_2 emitted), an upper purge ratio of 55.2% drastically decreases the energy penalty of the same bauxite, to 6.68% and 1.10 GJ per tonne of CO_2 avoided. This effect occurs in all three bauxite compositions studied, although to a lesser extent as the Al/Fe ratio becomes smaller. For instance, bauxite with a 1.5 Al/Fe ratio presents an energy penalty of 55.96% and 8.57 GJ/tonne $CO_{2\ \text{avoided}}$ when a low 2.6% purge ratio is carried out. These values are reduced at most to 17.76% and 2.79 GJ/tonne when a maximum purge of 44.2% is performed.

SPECCA indices obtained in this work, varying between a maximum of 8.57 and a minimum of 1.10 GJ/tonne $CO_{2\ \text{avoided}}$, fall within or above

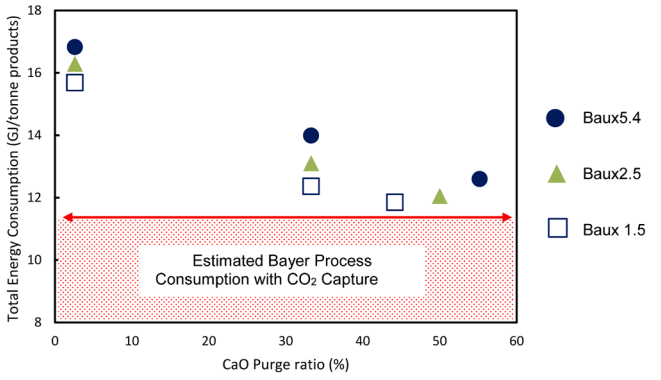

Fig. 8. Total energy consumption of integrated Pedersen and CO_2 Capture plants as a function of CaO purge ratio.

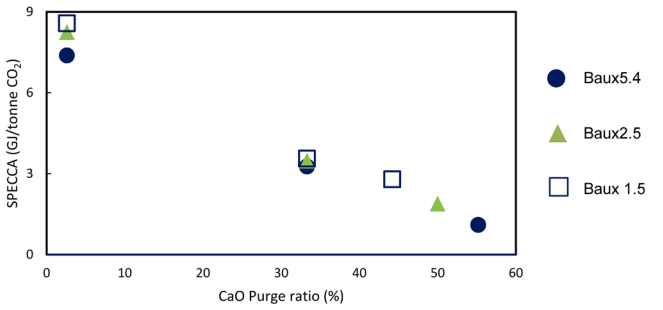

Fig. 9. SPECCA estimations as a function of CaO purge ratio.

the ranges reported in literature for CaL processes in other industrial sectors. As an example, SPECCA values of 4.45-7.27 GJ/tonne $CO_{2\ \text{avoided}}$ were obtained by studying the application of CaL plants in combined cycle power plants (Strojny et al., 2023) and values of 2.7-2.9 GJ/tonne $CO_{2\ \text{avoided}}$ were found when the integration of CaL plants in steelmaking industry was proposed (Perpiñán et al., 2023). More efficient configurations using indirectly heated calcium looping have demonstrated energy performance improvements and reduced penalties, with SPECCA values as low as 1.7–2.1 GJ/tonne CO_2 avoided in cement and lime applications (Ortiz et al., 2016) (Greco-Coppi et al., 2023). These results place the highest purge configurations of this study (1.10–2.79 GJ/tonne CO_2) within the competitive range of state-of-the-art CaL applications, while the low-purge configurations (7.38–8.57 GJ/tonne CO_2) are relatively high by comparison, especially at reduced CaO substitution levels. CaL integrations with low purge ratios present a minor grade of substitution of $CaCO_3$ in the Pedersen plant, and hence, higher SPECCA values are obtained. These values result slightly higher than SPECCA indices from other CaL integrations. However, when high purge ratios enable near-complete replacement of $CaCO_3$ by purged CaO, SPECCA values in this study are lowered to levels consistent with those obtained in optimized cement and lime CaL processes, which report values in the range of 0.57–2.17 GJ/tonne CO_2 avoided (Greco-Coppi et al., 2023) (Ferrario et al., 2023). The energy penalty reduction associated with high-purge operation highlights the potential of this configuration to approach or even outperform certain conventional CO_2 capture benchmarks in terms of energy efficiency.

Overall, using high spent CaO purge ratios shows a better performance than low purge ratios, mainly thanks to the use of $CaCO_3$ during the Pedersen process. When $CaCO_3$ was entirely replaced by CaO leaving the CaL unit, the global energy consumptions varied among 11.85-12.60 GJ per tonne of products, depending on the composition of bauxite. However, the energy penalty resulted too high to result viable when lower CaO purge ratios were proposed, boosting the energy demand to 15.85-16.99 GJ per tonne of products. Even when using the maximum purge ratios, and assuming that spent CaO is directly suitable for the formation of calcium-aluminate slags, the primary energy demand remains slightly higher than the estimated values of Bayer process plants with CO_2 capture, which show an energy demand of 11.35-11.54 GJ per tonne of alumina (Sáez-Guinoa et al., 2024). The additional advantage of bauxite residue avoidance manifests the potential relevance of combining these technologies for the decarbonisation and resource circularity objectives.

4. Conclusion

Throughout this study, an alternative route to extract alumina from bauxite was investigated, based on the principles of former industrial Pedersen process. Three case studies were carried out with different bauxites, varying the aluminium and iron content of the ores. The study consisted on the implementation of material and energy simulations and optimizations, using thermodynamic equilibriums and bibliographic

references as a basis for that purpose. The main conclusions found as results of the study are:

- The simulations resulted in the production of alumina and pig iron meeting the composition specifications of commercial products, and the generation of a grey mud containing over 60%wt of $CaCO_3$. Bauxite residues, occurring significantly in the standard industrial Bayer process, were avoided in all cases, entailing remarkable environmental benefits and better efficiencies in the use of resources.
- The global energy consumption, however, was found to be more intensive than Bayer process. This energy consumption, measured as energy demand per tonne of products, decreased as the aluminium/iron content ratio of the ore became smaller. Hence, bauxites with low Al/Fe ratios present a feasible energy consumptions, estimated between 10.15-10.93 GJ per tonne of products, whereas Bayer process average consumption stands at 10.22 GJ per tonne of alumina.
- The share of thermal and electric energy demand was also found to vary remarkably depending on the Al/Fe ratio of the ore. Bauxites with a low Al/Fe ratio presented a greater share of electricity demand. Thus, CO_2 emissions of the process were more sensitive to the carbon intensity of the electricity market. Hence, the availability of renewable electricity is a key aspect of the potential re-implementation of the industrial Pedersen process.

Another significant characteristic of the Pedersen process is the use of $CaCO_3$ to produce an intermediate slag, based primarily on $12CaO{\cdot}7Al_2O_3$. Higher Al/Fe ratios require higher amounts of $CaCO_3$, and, therefore, greater energy demands. The implementation of a CO_2 capture plant based on calcium-looping technology was proposed throughout this study to explore the potential advantages of integrating of CaO-$CaCO_3$. The main findings of this integration were:

- The substitution of $CaCO_3$ in the dehydration unit of the Pedersen plant by the injection of purged CaO from the CaL plant was the main factor affecting the performance of the CO_2 capture plant. Operating with high CaO purge ratios led to major substitution grades of $CaCO_3$, and, therefore, lesser energy penalties, improving the efficiency of the overall system.
- When using high CaO purge ratios, energy penalties were estimated to vary between 1.10-2.79 GJ per tonne of CO_2 avoided, obtaining values that fall within a range similar to those of industries that exploit the same $CaCO_3$-CaO integration (0.57–2.17 GJ/tonne CO_2 avoided), or similar to processes that use a more efficient indirectly heated calcium looping (1.7–2.1 GJ/tonne CO_2 avoided).
- The energy penalty of implementing the CO_2 capture resulted smaller as the Al/Fe ratio of the ore increased, because of the higher demand of $CaCO_3$ in those cases. However, overall energy demands remained lower for low Al/Fe ratios. The energy consumption, eliminating 98% of initial CO_2 direct emissions, was estimated at 11.85 and 12.05 GJ per tonne of products for 1.5 and 2.5 Al/Fe ratios respectively. These values were only slightly higher than estimated energy consumptions of CO_2 capture applied to Bayer process, showing a good basis for the continuance of studies in this direction.

The conducted study can entail discrepancies from real plants, due to the lack of industrial data and the technical assumptions that were made, such as the suitability of spent CaO sorbent from the CaL plant as feedstock, and the simplification of the kinetics and mechanisms of the slag digestion. Nonetheless, the findings of this work can encourage the search for innovative approaches to produce two critical raw materials such as alumina and pig iron. Such advancements could be an effective strategy for mitigating climate change impacts and addressing mineral resource scarcity.

The use of bauxites with low alumina content, which are more inefficient in the Bayer process, following alternative methods like the route explored in this work can play a relevant part in the decarbonisation of the industry and the avoidance of hazardous waste residues. In order to bring this technology closer to implementation, further experimental research may be necessary, especially to deepen the understanding of the digestibility of CaO-Al_2O_3 slags. Studies focusing on the chemical and physical behaviour of these slags will be essential to identify the key parameters influencing their reactivity. Additionally, large-scale experiments will be required to validate the practical feasibility and scalability of the proposed process, ensuring its performance under industrial conditions. Finally, the valorization of spent CaO sorbent from CaL processes and its use as raw material for the production of CaO-Al_2O_3 slags should be also regarded as a major research focus to achieve the potential benefits of the coupling of both technologies shown in this study.

CRediT authorship contribution statement

Javier Sáez-Guinoa: Writing – review & editing, Writing – original draft, Visualization, Software, Methodology, Formal analysis, Conceptualization. **Eva Llera-Sastresa:** Writing – review & editing, Supervision, Conceptualization. **Luis M Romeo:** Writing – review & editing, Supervision, Resources, Funding acquisition.

Declaration of competing interest

The authors declare that they have no known competing financial interests or personal relationships that could have appeared to influence the work reported in this paper.

Acknowledgements

The work described in this paper is supported by the Government of Aragon (Research Group DGA T46_23R: Energía y CO_2). Aspen Technology Inc. is also acknowledged for the use of the software.

Supplementary materials

Supplementary material associated with this article can be found, in the online version, at doi:10.1016/j.ijggc.2025.104453.

Data availability

Data will be made available on request.

References

Abanades, J.C., Anthony, E.J., Lu, D.Y., Salvador, C., Alvarez, D., 2004. Capture of CO2 from combustion gases in a fluidized bed of CaO. AIChE Journal 50, 1614–1622. https://doi.org/10.1002/aic.10132.

Alcoa – Refinery of the Future, (n.d.). https://www.alcoa.com/global/en/what-we-do/alumina/refinery-of-the-future (accessed March 13, 2024).

Alcoa to investigate low emissions alumina - Australian Renewable Energy Agency (ARENA), (n.d.). https://arena.gov.au/news/alcoa-to-investigate-low-emissions-alumina/(accessed March 13, 2024).

Amorim, A., Filipe, R.M., Matos, H.A., 2025. Analysis of integrated calcium looping alternatives in a cement plant. Chem Eng Sci 313, 121709. https://doi.org/10.1016/j.ces.2025.121709.

Arias, B., Alvarez Criado, Y., Méndez, A., Marqués, P., Finca, I., Abanades, J.C., 2024. Pilot Testing of Calcium Looping at TRL7 with CO2 Capture Efficiencies toward 99%. Energy & Fuels 38, 14757–14764. https://doi.org/10.1021/acs.energyfuels.4c02472.

Azof, F.I., Kolbeinsen, L., Safarian, J., 2018. Characteristics of Calcium-Aluminate Slags and Pig Iron Produced from Smelting-Reduction of Low-Grade Bauxites. Metallurgical and Materials Transactions B: Process Metallurgy and Materials Processing Science 49, 2400–2420. https://doi.org/10.1007/s11663-018-1353-1.

Azof, F.I., Vafeias, M., Panias, D., Safarian, J., 2020. The leachability of a ternary CaO-Al2O3-SiO2 slag produced from smelting-reduction of low-grade bauxite for alumina recovery. Hydrometallurgy 191. https://doi.org/10.1016/J.HYDROMET.2019.105184.

Banerjee, P.K., Mankar, A.U., Kumar, V., 2023. Beneficiation of bauxite ores. Mineral Processing. Elsevier, pp. 117–166. https://doi.org/10.1016/B978-0-12-823149-4.00014-4.

Bánvölgyi, G., Haneman, B., 2022. Chemical Processing of Bauxite: Alumina and Silica Minerals—Chemistry. Kinetics and Reactor Design 157–239. https://doi.org/10.1007/978-3-030-88586-1_4.

Barón, C., Perpiñán, J., Bailera, M., Peña, B., 2023. Techno-economic assessment of glassmaking decarbonization through integration of calcium looping carbon capture and power-to-gas technologies. Sustain Prod Consum 41, 121–133. https://doi.org/10.1016/J.SPC.2023.07.029.

Bogatyrev, B.A., Zhukov, V.V., 2009. Bauxite provinces of the world. Geology of Ore Deposits 51, 339–355. https://doi.org/10.1134/S1075701509050018.

Bond, F., 1961. Crushing and grinding calculations, Rev. ed. Allis-Chalmers Manufacturiing Co., Milwaukee Wis.

Conejo, A.N., 2024. Electric Arc Furnace: Methods to Decrease Energy Consumption. Springer Nature Singapore, Singapore. https://doi.org/10.1007/978-981-97-4053-6.

da C. Leite, R., Lucheta, A.R., Holanda, R.B., Silva, P.M.P., do Carmo, A.L.V., da C. Leite, R., de Melo, C.C.A., da Costa, R.V., Montini, M., Fernandes, A.R., 2022. Bauxite residue valorization — Soil conditioners production through composting with palm oil mill residual biomass. Science of The Total Environment 835, 155413. https://doi.org/10.1016/J.SCITOTENV.2022.155413.

Dentoni, V., Grosso, B., Massacci, G., 2014. Environmental sustainability of the alumina industry in Western Europe. Sustainability (Switzerland) 6, 9477–9493. https://doi.org/10.3390/su6129477.

Di Mare, M., Ouellet-Plamondon, C.M., 2023. Valorization of unmodified, filter-pressed bauxite residue as a precursor for alkali activated inorganic polymers in a one-part mixing process. J Clean Prod 386, 135658. https://doi.org/10.1016/J.JCLEPRO.2022.135658.

European Aluminium Association, VISION 2050 EUROPEAN ALUMINIUM'S CONTRIBUTION TO THE EU'S MID-CENTURY LOW-CARBON ROADMAP A vision for strategic, low carbon and competitive aluminium, (n.d.).

European Commission, Commission Delegated Regulation (EU) 2023/807 of 15 December 2022 on revising the primary energy factor for electricity in application of Directive 2012/27/EU of the European Parliament and of the Council, (2022).

European Environment Agency, 2023. Greenhouse gas emission intensity of electricity generation in Europe. https://www.eea.europa.eu/en/analysis/indicators/greenhouse-gas-emission-intensity-of-1. accessed May 7, 2024.

Evans, K., 2016. The History, Challenges, and New Developments in the Management and Use of Bauxite Residue. Journal of Sustainable Metallurgy 2, 316–331. https://doi.org/10.1007/S40831-016-0060-X/FIGURES/14.

Ferrario, D., Stendardo, S., Verda, V., Lanzini, A., 2023. Solar-driven calcium looping system for carbon capture in cement plants: Process modelling and energy analysis. J Clean Prod 394, 136367. https://doi.org/10.1016/J.JCLEPRO.2023.136367.

Georgala, E., Vafeias, M., Bempelou, A., Balomenos, E., Panias, D., 2023. Aluminium extraction from a calcium aluminate slag using sodium carbonate based on the critical examination of the patented industrial Pedersen process. Hydrometallurgy 222, 106188. https://doi.org/10.1016/J.HYDROMET.2023.106188.

Grasa, G.S., Abanades, J.C., 2006. CO2 capture capacity of CaO in long series of carbonation/calcination cycles. Ind Eng Chem Res 45, 8846–8851. https://doi.org/10.1021/ie0606946.

Greco-Coppi, M., Hofmann, C., Walter, D., Ströhle, J., Epple, B., 2023. Negative CO2 emissions in the lime production using an indirectly heated carbonate looping process. Mitig Adapt Strateg Glob Chang 28, 30. https://doi.org/10.1007/s11027-023-10064-7.

Greco-Coppi, M., Ströhle, J., Epple, B., 2025. Modeling and design of a calciner for commercial-scale CO2 capture using stochastic methods and results from pilot tests. Fuel 388. https://doi.org/10.1016/j.fuel.2024.133931.

Greco-Coppi, M., Ströhle, J., Epple, B., 2025. A carbonator model for CO2 capture based on results from pilot tests. Part II: Deactivation and reaction model. Chemical Engineering Journal 508, 159041. https://doi.org/10.1016/j.cej.2024.159041.

Guo, X., Zhou, W., Wei, J., 2024. Numerical simulation of fluidized bed reactor for calcium looping energy release process in thermochemical storage: Influence of key conditions. Renew Energy 237, 121532. https://doi.org/10.1016/J.RENENE.2024.121532.

Haaf, M., Anantharaman, R., Roussanaly, S., Ströhle, J., Epple, B., 2020. CO2 capture from waste-to-energy plants: Techno-economic assessment of novel integration concepts of calcium looping technology. Resour Conserv Recycl 162, 104973. https://doi.org/10.1016/J.RESCONREC.2020.104973.

Haaf, M., Hilz, J., Peters, J., Unger, A., Ströhle, J., Epple, B., 2020. Operation of a 1 MWth calcium looping pilot plant firing waste-derived fuels in the calciner. Powder Technol 372, 267–274. https://doi.org/10.1016/j.powtec.2020.05.074.

Hanak, D.P., Anthony, E.J., Manovic, V., 2015. A review of developments in pilot-plant testing and modelling of calcium looping process for CO2 capture from power generation systems. Energy Environ Sci 8, 2199–2249. https://doi.org/10.1039/C5EE01228G.

Haran, S., Rao, A.B., Banerjee, R., 2023. Life cycle energy-carbon-water footprint assessment of an existing coal power plant retrofitted with calcium looping (CaL) based CCS system. International Journal of Greenhouse Gas Control 130, 104015. https://doi.org/10.1016/J.IJGGC.2023.104015.

Harvey, L.D.D., 2024. A bottom-up assessment of recent (2016–20) energy use by the global iron and steel industry constrained to match a top-down (International Energy Agency) assessment. Energy 293, 130675. https://doi.org/10.1016/J.ENERGY.2024.130675.

He, S., Zeng, X., Zheng, Y., Zhu, M., Wang, D., Wang, J., 2025. Thermodynamic analysis of decarbonizing NGCC power plants by the tail-end green ammonia-driven calcium looping. Energy 314, 134147. https://doi.org/10.1016/J.ENERGY.2024.134147.

Hejazi, B., Grace, J.R., 2020. Simulation of tar-free biomass syngas enhancement in a calcium looping operation using Aspen Plus built-in fluidized bed model. International Journal of Greenhouse Gas Control 99, 103096. https://doi.org/10.1016/J.IJGGC.2020.103096.

Hejazi, B., Montagnaro, F., 2024. A Modeling and Simulation Study to Accommodate Sorbent Sintering in a Ca-Looping System Coupled with a Cement Plant. Ind Eng Chem Res 63, 11069–11081. https://doi.org/10.1021/acs.iecr.4c00941.

Holanda, R.B., Silva, P.M.P., do Carmo, A.L.V., Cardoso, A.F., da Costa, R.V., de Melo, C. C.A., Lucheta, A.R., Montini, M., 2020. Bayer Process Towards the Circular Economy—Soil Conditioners from Bauxite Residue, Minerals. Metals and Materials Series 107–114. https://doi.org/10.1007/978-3-030-36408-3_15/COVER.

Hornberger, M., Spörl, R., Scheffknecht, G., 2017. Calcium Looping for CO2 Capture in Cement Plants – Pilot Scale Test. Energy Procedia 114, 6171–6174. https://doi.org/10.1016/j.egypro.2017.03.1754.

Hudson, L.K., Misra, C., Perrotta, A.J., Wefers, K., Williams, F.S., 2012. Aluminum Oxide. Ullmann's Encyclopedia of Industrial Chemistry, 2nd ed., pp. 607–644. https://doi.org/10.1002/14356007.a01_557

International Aluminium, Alumina Production - International Aluminium, (n.d.). https://international-aluminium.org/statistics/alumina-production/(accessed April 19, 2024).

International Aluminium Institute [IAI], World Aluminium, (n.d.).

International Energy Agency, Energy Technology Perspectives 2020, Energy Technology Perspectives 2020 (2020). https://doi.org/10.1787/ab43a9a5-en.

International Energy Agency, Energy Technology Perspectives 2023, Energy Technology Perspectives 2023 (2023). https://doi.org/10.1787/7C6B23DB-EN.

Jackson, S., Brodal, E., 2019. Optimization of the energy consumption of a carbon capture and sequestration related carbon dioxide compression processes. Energies (Basel) 12. https://doi.org/10.3390/en12091603.

Jiang, D., Li, S., Santasalo-Aarnio, A., Järvinen, M., 2024. Aspen plus-based techno-economic assessment of a solar-driven calcium looping CO2 capture system integrated with CaO sorbent reactivation. Energy Conversion and Management: X 23, 100673. https://doi.org/10.1016/J.ECMX.2024.100673.

JRC Reference Reports, Best Available Techniques (BAT) Reference Document for the Production of Cement, Lime and Magnesium Oxide, 2013.

Kaczyńska, K., Kaczyński, K., Pełka, P., 2021. Calcination of Clay Raw Materials in a Fluidized Bed. Materials 14, 3989. https://doi.org/10.3390/ma14143989.

Kar, M.K., Önal, M.A.R., Borra, C.R., 2023. Alumina recovery from bauxite residue: A concise review. Resour Conserv Recycl 198, 107158. https://doi.org/10.1016/J.RESCONREC.2023.107158.

Keplinger, T., Haider, M., Steinparzer, T., Patrejko, A., Trunner, P., Haselgrübler, M., 2018. Dynamic simulation of an electric arc furnace waste heat recovery system for steam production. Appl Therm Eng 135, 188–196. https://doi.org/10.1016/J.APPLTHERMALENG.2018.02.060.

Königsberger, E., 2008. Thermodynamic simulation of the Bayer process. Zeitschrift Fuer Metallkunde/Materials Research and Advanced Techniques 99, 197–202. https://doi.org/10.3139/146.101624.

Konlechner, D., Koenig, R., Preveniou, A., Davris, P., Balomenos, E., 2021. First Industrial Scale Process Concept for the Reengineered Pedersen Process within ENSUREAL. Materials Proceedings 5, 8. https://doi.org/10.3390/MATERPROC2021005008, 2021Vol. 5, Page 8.

Lazou, A., van der Eijk, C., Balomenos, E., Kolbeinsen, L., Safarian, J., 2020. On the Direct Reduction Phenomena of Bauxite Ore Using H2 Gas in a Fixed Bed Reactor. Journal of Sustainable Metallurgy 6, 227–238. https://doi.org/10.1007/S40831-020-00268-5/FIGURES/13.

Li, G., Liu, J., Yi, L., Luo, J., Jiang, T., 2024. Bauxite residue (red mud) treatment: Current situation and promising solution. Science of The Total Environment 948, 174757. https://doi.org/10.1016/J.SCITOTENV.2024.174757.

Liu, W., Yang, J., Xiao, B., 2009. Review on treatment and utilization of bauxite residues in China. Int J Miner Process 93, 220–231. https://doi.org/10.1016/J.MINPRO.2009.08.005.

Liu, X., Jin, K., Li, X., Yang, R., 2023. Low-carbon cement manufacturing enabled by electrified calcium looping and thermal energy storage. International Journal of Greenhouse Gas Control 129, 103986. https://doi.org/10.1016/J.IJGGC.2023.103986.

Ma, Y., Preveniou, A., Kladis, A., Pettersen, J.B., 2022. Circular economy and life cycle assessment of alumina production: Simulation-based comparison of Pedersen and Bayer processes. J Clean Prod 366, 132807. https://doi.org/10.1016/J.JCLEPRO.2022.132807.

Martínez, A., Lara, Y., Lisbona, P., Romeo, L.M., 2012. Energy penalty reduction in the calcium looping cycle. International Journal of Greenhouse Gas Control 7, 74–81. https://doi.org/10.1016/J.IJGGC.2011.12.005.

Metallurgical Alumina Refining Energy Intensity - International Aluminium Institute, (n.d.). https://international-aluminium.org/statistics/metallurgical-alumina-refining-energy-intensity/(accessed March 12, 2024).

Miller, J., Irgens, A., 2013. Alumina production by the Pedersen process - Hystory and future. In: Donaldson, D., Raahauge, B.E. (Eds.), Essential Readings in Light Metals: Alumina and Bauxite, The Minera. John Wiley & Sons, Inc., pp. 977–982

Ortiz, C., Valverde, J.M., Chacartegui, R., 2016. Energy Consumption for CO2 Capture by means of the Calcium Looping Process: A Comparative Analysis using Limestone, Dolomite, and Steel Slag. Energy Technology 4, 1317–1327. https://doi.org/10.1002/ENTE.201600390.

Pascual, S., Lisbona, P., Bailera, M., Romeo, L.M., 2021. Design and operational performance maps of calcium looping thermochemical energy storage for concentrating solar power plants. Energy 220, 119715. https://doi.org/10.1016/J.ENERGY.2020.119715.

H. Pedersen, Process for the Manufacture of Aluminium Oxide, GB1308626A, 1927.

Peppas, A., Politi, C., Kottaridis, S., Taxiarchou, M., 2023. LCA Analysis Decarbonisation Potential of Aluminium Primary Production by Applying Hydrogen and CCUS Technologies. Hydrogen 4, 338–356. https://doi.org/10.3390/hydrogen4020024.

Perejón, A., Romeo, L.M., Lara, Y., Lisbona, P., Martínez, A., Valverde, J.M., 2016. The Calcium-Looping technology for CO2 capture: On the important roles of energy integration and sorbent behavior. Appl Energy 162, 787–807. https://doi.org/10.1016/J.APENERGY.2015.10.121.

Perpiñán, J., Bailera, M., Peña, B., 2023. Full oxygen blast furnace steelmaking: From direct hydrogen injection to methanized BFG injection. Energy Convers Manag 295, 117611. https://doi.org/10.1016/J.ENCONMAN.2023.117611.

Perpiñán, J., Peña, B., Bailera, M., Eveloy, V., Kannan, P., Raj, A., Lisbona, P., Romeo, L. M., 2023. Integration of carbon capture technologies in blast furnace based steel making: A comprehensive and systematic review. Fuel 336, 127074. https://doi.org/10.1016/J.FUEL.2022.127074.

Pilla, G., Hertel, T., Douvalis, A.P., Kapelari, S., Blanpain, B., Pontikes, Y., 2024. Towards sustainable valorization of bauxite residue: Thermodynamic analysis, comprehensive characterization, and response surface methodology of H2 reduced products for simultaneous metal recovery. J Clean Prod 440, 140931. https://doi.org/10.1016/J.JCLEPRO.2024.140931.

Porrazzo, R., White, G., Ocone, R., 2014. Aspen Plus simulations of fluidised beds for chemical looping combustion. Fuel 136, 46–56. https://doi.org/10.1016/J.FUEL.2014.06.053.

Rodriguez, N., Alonso, M., Grasa, G., Abanades, J.C., 2008. Heat requirements in a calciner of CaCO3 integrated in a CO2 capture system using CaO. Chemical Engineering Journal 138, 148–154. https://doi.org/10.1016/J.CEJ.2007.06.005.

Romano, M.C., 2012. Modeling the carbonator of a Ca-looping process for CO2 capture from power plant flue gas. Chem Eng Sci 69, 257–269. https://doi.org/10.1016/j.ces.2011.10.041.

Romeo, L.M., Abanades, J.C., Escosa, J.M., Paño, J., Giménez, A., Sánchez-Biezma, A., Ballesteros, J.C., 2008. Oxyfuel carbonation/calcination cycle for low cost CO2 capture in existing power plants. Energy Convers Manag 49, 2809–2814. https://doi.org/10.1016/J.ENCONMAN.2008.03.022.

Romeo, L.M., Catalina, D., Lisbona, P., Lara, Y., Martínez, A., 2011. Reduction of greenhouse gas emissions by integration of cement plants, power plants, and CO2 capture systems. Greenhouse Gases: Science and Technology 1, 72–82. https://doi.org/10.1002/GHG3.5.

Romeo, L.M., Lara, Y., Lisbona, P., Escosa, J.M., 2009. Optimizing make-up flow in a CO2 capture system using CaO. Chemical Engineering Journal 147, 252–258. https://doi.org/10.1016/j.cej.2008.07.010.

A. Ruys, Refining of alumina: The Bayer process, Alumina Ceramics (2019) 49–70. https://doi.org/10.1016/B978-0-08-102442-3.00003-8.

Saevarsdottir, G., Kvande, H., Welch, B.J., 2020. Aluminum Production in the Times of Climate Change: The Global Challenge to Reduce the Carbon Footprint and Prevent Carbon Leakage. Jom 72, 296–308. https://doi.org/10.1007/s11837-019-03918-6.

Sáez-Guinoa, J., García-Franco, E., Llera-Sastresa, E., Romeo, L.M., 2024. The effects of energy consumption of alumina production in the environmental impacts using life cycle assessment. International Journal of Life Cycle Assessment 29, 380–393. https://doi.org/10.1007/S11367-023-02257-8.

Sáez-Guinoa, J., Senante, I., Llera-Sastresa, E., Romeo, L.M., 2024. Techno-economic assessment of solar photovoltaic electrification and calcium looping technology as decarbonisation pathways of alumina industry. Results in Engineering 23, 102456. https://doi.org/10.1016/J.RINENG.2024.102456.

Sáez-Guinoa, J., Senante, I., Pascual, S., Llera-Sastresa, E., Romeo, L.M., 2024. Eco-efficiency assessment of carbon capture and hydrogen transition as decarbonisation strategies in alumina production. J Clean Prod 485, 144366. https://doi.org/10.1016/j.jclepro.2024.144366.

Safarian, J., Kolbeinsen, L., 2016. Smelting-reduction of Bauxite for Sustainable Alumina Production. Sustainable Industrial Processing Summit and Exhibition 5, 149–158.

Salim, M.U., Mosaberpanah, M.A., Danish, A., Ahmad, N., Khalid, R.A., Moro, C., 2023. Role of bauxite residue as a binding material and its effect on engineering properties of cementitious Composites: A review. Constr Build Mater 409, 133844. https://doi.org/10.1016/J.CONBUILDMAT.2023.133844.

Sattari, F., Tahmasebpoor, M., Valverde, J.M., Ortiz, C., Mohammadpourfard, M., 2021. Modelling of a fluidized bed carbonator reactor for post-combustion CO2 capture considering bed hydrodynamics and sorbent characteristics. Chemical Engineering Journal 406, 126762. https://doi.org/10.1016/j.cej.2020.126762.

Sellaeg, H., Kolbeinsen, L., Safarian, J., 2017. Iron Separation from Bauxite Through Smelting-Reduction Process. Minerals, Metals and Materials Series 0, 127–135. https://doi.org/10.1007/978-3-319-51541-0_19.

Shafiabadi, A., Hejazi, B., Manovic, V., 2025. Studying the effect of sorbent sintering in the thermodynamic simulations of sorption enhanced chemical looping steam methane reforming. Fuel 401, 135858. https://doi.org/10.1016/j.fuel.2025.135858.

Shimizu, T., Hirama, T., Hosoda, H., Kitano, K., Inagaki, M., Tejima, K., 1999. A Twin Fluid-Bed Reactor for Removal of CO2 from Combustion Processes. Chemical Engineering Research and Design 77, 62–68. https://doi.org/10.1205/026387699525882.

Sidrak, Y.L., 2001. Dynamic simulation and control of the bayer process. A review. Ind Eng Chem Res 40, 1146–1156. https://doi.org/10.1021/ie000522n.

Ströhle, J., Hilz, J., Epple, B., 2020. Performance of the carbonator and calciner during long-term carbonate looping tests in a 1 MWth pilot plant. J Environ Chem Eng 8, 103578. https://doi.org/10.1016/J.JECE.2019.103578.

Strojny, M., Gładysz, P., Hanak, D.P., Nowak, W., 2023. Comparative analysis of CO2 capture technologies using amine absorption and calcium looping integrated with natural gas combined cycle power plant. Energy 284, 128599. https://doi.org/10.1016/J.ENERGY.2023.128599.

Swain, B., Lee, C.G., Park, J.R., 2022. Assessment of bauxite residue as secondary resource for rare earth metal and valorization challenges: A perspective. Resources, Conservation & Recycling Advances 14, 200078. https://doi.org/10.1016/J.RCRADV.2022.200078.

The European Green Deal - European Commission, (n.d.). https://commission.europa.eu/strategy-and-policy/priorities-2019-2024/european-green-deal_en (accessed April 19, 2024).

United Nations Environment Programme, 2024. Global Resources Outlook 2024.

Vafeias, M., Marinos, D., Panias, D., Safarian, J., Van Der Eijk, C., Solheim, I., Balomenos, E., Ksiazek, M., Davris, P., 2018. From red to grey: revisiting the Pedersen process to achieve holistic bauxite ore utilisation. In: 2nd International Bauxite Residue Valorisation and Best Practices Conference, pp. 111–117.

Yang, Y., Tao, W., Liu, W., Hu, X., Wang, Z., Shi, Z., Shu, X., 2020. The Adsorption Behavior of Moisture on Smelter Grade Alumina during Transportation and Storage—for Primary Aluminum Production. Metals (Basel) 10, 325. https://doi.org/10.3390/met10030325.

Yao, J.G., Zhang, Z., Sceats, M., Maitland, G.C., Fennell, P.S., 2017. Two-Phase Fluidized Bed Model for Pressurized Carbonation Kinetics of Calcium Oxide. Energy & Fuels 31, 11181–11193. https://doi.org/10.1021/acs.energyfuels.7b01384.

Zainudeen, N.M., Mohammed, L., Nyamful, A., Adotey, D., Osae, S.K., 2023. A comparative review of the mineralogical and chemical composition of African major bauxite deposits. Heliyon 9, e19070. https://doi.org/10.1016/J.HELIYON.2023.E19070.

Zhang, Y., Wang, Y., Han, K., Zhao, J., Wu, J.J., Li, Y., 2024. Calcium looping for CO2 capture and thermochemical heat storage, a potential technology for carbon neutrality: A review. Green Energy and Resources 2, 100078. https://doi.org/10.1016/J.GERR.2024.100078.

Zhou, G.T., Wang, Y.L., Qi, T.G., Zhou, Q.S., Liu, G.H., Peng, Z.H., Li, X.Bin, 2023. Toward sustainable green alumina production: A critical review on process discharge reduction from gibbsitic bauxite and large-scale applications of red mud. J Environ Chem Eng 11, 109433. https://doi.org/10.1016/J.JECE.2023.109433.